

Electrocatalysis-driven sustainable plastic waste upcycling

Gaihong Wang¹ | Zhijie Chen²  | Wei Wei¹ | Bing-Jie Ni²

¹Centre for Technology in Water and Wastewater, School of Civil and Environmental Engineering, University of Technology Sydney, Sydney, New South Wales, Australia

²UNSW Water Research Centre, School of Civil and Environmental Engineering, The University of New South Wales, Sydney, New South Wales, Australia

Correspondence

Zhijie Chen and Bing-Jie Ni.
Email: zhijie.chen1@unsw.edu.au and bingjieni@gmail.com

Funding information

Australian Research Council, Grant/Award Number: DP220101139

Abstract

With large quantities and natural resistance to degradation, plastic waste raises growing environmental concerns in the world. To achieve the upcycling of plastic waste into value-added products, the electrocatalytic-driven process is emerging as an attractive option due to the mild operation conditions, high reaction selectivity, and low carbon emission. Herein, this review provides a comprehensive overview of the upgrading of plastic waste via electrocatalysis. Specifically, key electrooxidation processes including the target products, intermediates and reaction pathways in the plastic electro-reforming process are discussed. Subsequently, advanced electrochemical systems, including the integration of anodic plastic monomer oxidation and value-added cathodic reduction and photo-involved electrolysis processes, are summarized. The design strategies of electrocatalysts with enhanced activity are highlighted and catalytic mechanisms in the electrocatalytic oxidation of plastic waste are elucidated. To promote the electrochemistry-driven sustainable upcycling of plastic waste, challenges and opportunities are further put forward.

KEYWORDS

catalyst design, electrocatalytic reforming, electrochemical oxidation, hydrogen energy, plastic waste

1 | INTRODUCTION

Due to the advantages of low price, light weight, and excellent durability, plastics have been regarded as indispensable materials in ever-expanding applications.¹ Based on the molecular structure, plastics could be classified into polyethylene terephthalate (PET), polystyrene, polypropylene, high-density polyethylene, low-density polyethylene, polyvinyl chloride, polylactic acid (PLA), poly(methyl methacrylate) (PMMA), polybutylene terephthalate (PBT), and polyethylene furanoate (PEF), etc.² In 2022, the Organization for Economic Co-operation and Development reported that the global annual plastic production increased from 234 million tons in 2000 to

460 million tons in 2019 and it is estimated to triple to 1.231 billion metric tons in 2060. In 2019, nearly 70% of plastic waste was disposed through the landfill and incineration and only 9% of plastic waste was efficiently recovered. Nevertheless, over 20% of plastic waste was directly discarded into the natural environment.³ The spontaneous degradation of plastic waste under natural conditions could take hundreds or even thousands of years, which would not only lay a heavy burden on the ecosystem but also aggravate global environmental contamination.^{4–8} For example, the entire lifecycle of plastics may increase greenhouse gas emissions, thus triggering a grimmer global warming crisis. Furthermore, more seriously, under decomposition such as photolysis or microbial,

This is an open access article under the terms of the [Creative Commons Attribution](https://creativecommons.org/licenses/by/4.0/) License, which permits use, distribution and reproduction in any medium, provided the original work is properly cited.

© 2024 The Authors. *Electron* published by Harbin Institute of Technology and John Wiley & Sons Australia, Ltd.

plastic waste would be fragmented into microplastics (MPs) which are considered as highly hazardous pollutants.^{9–12} Therefore, it is indispensable to properly dispose the plastic waste to cut off the source of MPs, thereby relieving the global environment crisis and alleviating the negative effect on human health.

Up to now, multiple technologies have been applied for plastic waste recycling, including mechanical process, thermochemical depolymerization, advanced oxidation processes (AOPs), photocatalysis, electrocatalysis, and biological enzymolysis.^{13–18} Mechanical recycling is a primary way to manage plastic waste through a sequence of steps such as collection, separation and gridding.^{19,20} Regenerated materials by this way suffer from serious performance deterioration, defined as downcycling products.²¹ Typical plastic depolymerization by the thermochemical method commonly includes hydrolysis, glycolysis, hydrogenolysis, aminolysis, and diaminolysis.^{14,22–25} Such thermochemical depolymerization methods not only require high temperature and pressure but also involve harmful organic solvents and even expensive hydrogen.^{26–28} Biological enzymolysis is regarded as an environment-friendly way to decompose the waste plastic while raw plastic materials are substantially mineralized into CO₂ and H₂O rather than valuable monomers that could be put into the industrial applications. Similarly, AOPs are solely limited to the degradation of plastic materials by reactive oxygen species but could not realize the high-value conversion of plastic waste. Photocatalysis is considered as an eco-friendly method to convert plastic into diverse products, but the process takes a relatively long period and complex product composition. Alternatively, electrochemical reforming has attracted considerable attention due to the renewable energy-driven abundant electricity supply, mild operational conditions, high reaction efficiency, and product valorization with high selectivity.^{29–31}

In the conventional electrochemical process of water splitting, an external electric current is employed to facilitate electro-redox reactions at the interface of the electrolyte and electrode. Specifically, the hydrogen evolution reaction (HER) unfolds at the cathode, resulting in the liberation of hydrogen gas, while the oxygen evolution reaction (OER) at the anode leads to the release of oxygen gas.^{32–36} The four-electron OER at the anode requires a high overpotential due to its sluggish kinetics, thereby reducing the electrocatalytic efficiency.^{37–41} During the process of water splitting, relatively high energy (at least 1.6 V) beyond the theoretical energy input (1.23 V) is demanded for driving the overall electrocatalytic reactions.⁴² To tackle this issue, thermodynamically more favorable oxidation reactions have been explored to replace OER, such as alcohol

oxidation,^{43,44} urea oxidation,^{45–47} biomass oxidation,^{48,49} and 5-(hydroxymethyl)furfural (HMF) oxidation.^{50,51} In this context, plastic oxidation is also emerging as an attractive alternative to OER with the advantages of less energy input and waste utilization. In comparison with OER, an applied potential to drive plastic oxidation reaction and achieve a targeted current density shows a significant decrease, suggesting diminished energy contribution in the electrocatalytic system of plastic oxidation coupled with HER than water splitting system.⁵² For example, Liu et al.⁵³ compared the electricity consumption for the hydrogen production in the aforementioned systems and revealed that at a current density of 100 mA cm⁻², the plastic oxidation coupled with the HER system exhibited a markedly lower electricity consumption of 24.9 kWh kg⁻¹ (H₂), half of that for conventional water splitting system. Plastic electrochemical oxidation reactions typically occur in alkaline environments, concurrently engaging various cathodic reduction reactions, such as the HER, carbon dioxide reduction reaction (CO₂RR), and nitrate reduction reaction (NO₃RR). These integration systems not only contribute to the degradation of plastic but also enable the generation of valuable products, such as hydrogen and reduced carbon or nitrogen species. Additionally, the incorporation of photocatalysis into plastic electrochemical oxidation systems serves to augment their efficiency and broaden their applicability.

The current research on electrocatalysis-driven plastic waste upgrading primarily centers on PET plastic waste. In this process, PET undergoes hydrolysis under alkaline conditions, leading to the transformation of PET into ethylene glycol (EG) and either terephthalate (TPA) or purification of terephthalic acid (PTA) (Figure 1A).^{1,56,57} Subsequently, TPA can be extracted from the hydrolyzate as a raw material for the production of new PET.⁵⁸ By the end of 2021, the market of EG was projected to witness an output of around 24.95 million tons, with total market consumption reaching approximately 25.61 million tons, leading to a state of equilibrium between market supply and demand. Concurrently, the demand for EG, a pivotal platform molecule mainly for the production of PET, is foreseen to decline further, influenced by the growing global preference for biodegradable plastics. In light of this, the electrochemical valorization of EG emerges as an opportunity for the generation of value-added chemicals, as opposed to direct physical recovery. EG can undergo the oxidation reaction at the anode, resulting in the production of C1 (e.g., formic acid [FA]) and/or C2 (e.g., glycolic acid [GA]) products. As of reports in 2017, the global supply and demand for FA were largely in equilibrium, with actual output at approximately 700,000 tons and expected demand at

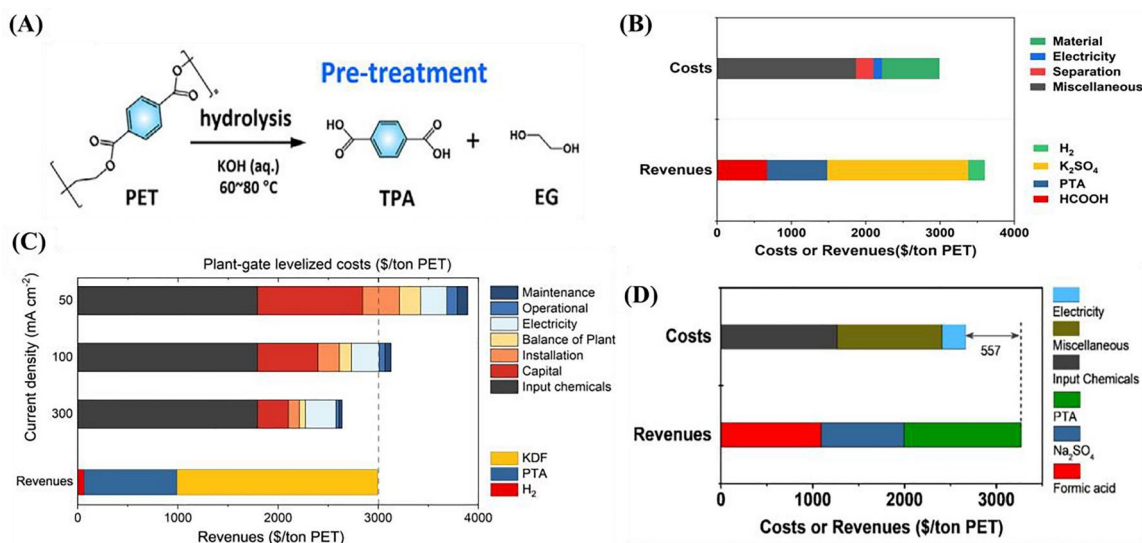


FIGURE 1 Conceptual design. (A) Hydrolysis of PET into TPA and EG. Reproduced with permission.¹ Copyright 2023, Elsevier. (B) TEA of the electrocatalytic upcycling process to transform PET plastic waste into valued chemicals, HCOOH, PTA, H₂ and K₂SO₄. (C) TEA of electrocatalytic PET upcycling to commodity chemicals and H₂ fuel at different current densities. Reproduced with permission.⁵⁴ Copyright 2021, Spring Nature. (D) TEA of the electrocatalytic upcycling process to transform PET plastic waste into valued chemicals, formic acid, PTA and Na₂SO₄. Reproduced with permission.⁵⁵ Copyright 2022, American Chemical Society. EG, ethylene glycol; KDF, potassium diformate; PET, polyethylene terephthalate; PTA, terephthalic acid; TEA, techno-economic analysis; TPA, terephthalate.

around 670,000 tons. Nevertheless, in response to environmental concerns, companies involved in FA production are encouraged to prioritize the sustainability of their processes and promote the development of more environmentally friendly products. In 2022, the market size of GA, valued at approximately US\$100–300 per kg,^{59,60} reaching ~US\$1 billion. This market is anticipated to escalate to US\$4 billion by 2035, fueled by the rising demand for products like cosmetics and degradable plastics. This underscores the feasibility of the electrochemical conversion of EG into C1 and C2 products as a viable strategy to align with market demands and enhance overall product value. Moreover, comprehensive techno-economic analyses (TEAs) have been conducted to assess the viability of the systems coupling ethylene glycol oxidation reaction (EGOR) with cathodic reduction reactions to co-produce valuable products. As illustrated in Figure 1B, the coupling system of EGOR with HER demonstrated a net revenue of \$614 per ton of PET at a cell voltage of 1.5 V, confirming its profitability.⁶¹ Of note, targeted enhancements to product quality have the potential to further optimize the profitability of the electrocatalytic system for upcycling plastic waste. For instance, the conversion of FA into potassium diformate (KDF), an emerging commodity product, led to a revenue increase of about \$1250.⁵⁴ Considering the plant-gate levelized costs, the estimated net revenues for upcycling one ton of waste PET amounted to ~\$350 at a commercially relevant current density (>300 mA cm⁻²) (Figure 1C). Additionally, in the EGOR coupling system with CO₂RR for FA production, an initial TEA indicated a substantial

net revenue of approximately \$557 per ton of PET, demonstrating the economic feasibility of converting PET plastic and CO₂ waste into valuable chemicals.⁵⁵ Besides PET-derived EG, the electrooxidation of other plastic (e.g., PBT, PEF, PE)-derived monomers also attracts growing interest and generated products (e.g., succinic acid) have been demonstrated to possess significant value.⁶²

In electrochemical reactions, the significance of electrocatalysts lies in their crucial role in accelerating reaction rates, lowering activation energies, enhancing selectivity, improving efficiency, and ensuring stability.^{63–67} Notably, their impacts on EGOR selectivity toward C1 or C2 products stand out in the electrochemical process of PET. Transition metal-based catalysts demonstrate efficacy in the electrochemical conversion of EG into C1 products, while noble metal-based electrocatalysts exhibit exceptional catalytic activity favoring C2 products.^{53,55,68,69} Consequently, achieving high selectivity for either C1 or C2 products necessitates the meticulous design of electrocatalysts with outstanding performance. Modification strategies are essential for augmenting the performance of electrocatalysts.⁷⁰ These strategies encompass tuning the composition through techniques such as doping or alloying, introducing active sites through surface functionalization, nanostructuring for increased surface area, and incorporating heteroatoms.^{71–74}

In this review, we illuminate recent advances in the field of the electrocatalysis-driven upcycling of plastic waste. Firstly, we introduce the key electrochemical processes involved in plastic electro-

upcycling, especially the C1 and C2 reaction pathways of EGOR. Afterward, we systematically summarize the integration systems that combine plastic electro-upcycling with HER, CO₂RR, and NO₃⁻RR, as well as photoelectrochemical (PEC) systems. Therefore, the electrocatalytic performances of such advanced systems are evaluated. We place special emphasis on the design strategies of electrocatalysts, aiming at expanding current understanding of high-performance catalyst design. Eventually, challenges and opportunities for the boost of plastic waste upcycling into high-value chemicals/fuels through the electrochemical approach are discussed.

2 | KEY ELECTROOXIDATION PROCESSES IN PLASTIC ELECTRO-REFORMING

2.1 | PET electrooxidation processes

Prior to the electro-reforming process, PET undergoes hydrolysis, resulting in the production of hydrolyzate containing TPA and EG. Various advanced hydrolysis technologies, such as neutral hydrolysis,⁷⁵ enzymatic hydrolysis,⁷⁶ acid hydrolysis,⁷⁷ and alkaline hydrolysis,⁷⁸ have been explored.⁷⁹ Among these, alkaline hydrolysis has gained significant attention due to its advantages of low cost and high TPA purity. The efficiency of alkaline hydrolysis can be substantially enhanced by optimizing reaction conditions, including the use of catalysts,⁷⁸ microwave assistance,⁸⁰ and the introduction of ethanol solvent.⁸¹ The outcome of the PET hydrolysis process is intricately linked to specific parameters related to PET, encompassing the type, source, and particle size.⁸² Additionally, crucial reaction parameters, including temperature, NaOH amount, PET concentration, stirring speed, and reaction time, play pivotal roles in determining both the yield and purity of the targeted products, such as TPA and EG.^{82–84}

2.1.1 | C1 pathway

FA or formate, is a representative C1 product with diverse applications in the production of leather, fiber, and rubber.⁸⁵ Traditionally, the synthesis of FA involves the chemical oxidation of fossil feedstocks under elevated temperatures and pressures, leading to substantial energy consumption.⁸⁶ In response to the imperative to minimize energy usage and environmental impact, significant attention has been directed toward electrochemical processes for FA production.^{87,88} Researchers have been actively exploring electrochemical pathways to derive FA from EG.

EG to FA or formate typically proceeds through a series of oxidation reactions.^{60,89} Initially, *EG was formed by the adsorption of EG on the surface of catalysts, followed by the formation of *glycolaldehyde. Afterward, *glyoxal was observed as the major intermediate, which was supported by the peak at 1110 cm⁻¹ formed in the in situ Fourier transform infrared (FTIR) spectra (Figure 2A).⁶¹ Although the peaks attributed to COO⁻ from GA was found, *GA was proved to be a minor intermediate due to its higher free energy change from *glycolaldehyde (1.30 eV) than that of *glyoxal (1.08 eV). Finally, *Formate was mainly produced from the *glyoxal, identified by a large amount of formate presented by nuclear magnetic resonance (NMR) spectra and in situ FTIR spectroscopy. Although the intermediate of glycolaldehyde is hardly detected due to the fast reaction, Liu et al.⁹⁰ proved the presence of *glycolaldehyde (*CH₂OHCHO) through the in situ FTIR spectra (Figure 2B), which was assigned to the peak at 1740 cm⁻¹. Nevertheless, *CH₂OHCHO was further oxidized into *CH₂O and *HCOOH, indicating another possible reaction pathway originated from *glycolaldehyde. Subsequently, *CH₂O was transformed into and *HCOOH via the Cannizzaro reaction, evidenced by the peak at 1430 cm⁻¹ assigned to the OH bending vibration of methanol in in situ FTIR spectra. Next, *CH₃OH was further oxidized into FA.

Another pathway to generate the FA was proposed by Wang et al. (Figure 2C).⁹¹ In their study, *OHCH₂-H₂CHO* (*EG) was firstly converted to *OCH₂-CH₂O* by breaking all of the O-H_α bonds rather than *OCH-H₂CHO*, because the formation of the former is an exothermic process while that of the latter is an endothermic process. Sequentially, *OCH₂-CH₂O* broke all the C-H_β bonds to form the *OCH-HCO*, which may be altered to GA under the alkaline condition via the Cannizzaro reaction, since the high-performance liquid chromatography (HPLC) chromatogram verified the existence of GA. Finally, FA was generated from the C-C bond cleavage of the *OCH-HCO*.

2.1.2 | C2 pathway

GA (glycolate under base condition), a partially oxidized C2 compound, has been extensively applied in various fields as an important chemical commodity, especially used as a building block for the production of degradable plastics.⁹² Traditional synthesis of GA is mainly from coal-based chemicals, which accelerated the consumption of nonrenewable resources. Therefore, more sustainable approaches are in great demand, such as clean electrochemical processes. Although the formation of C2 products is not

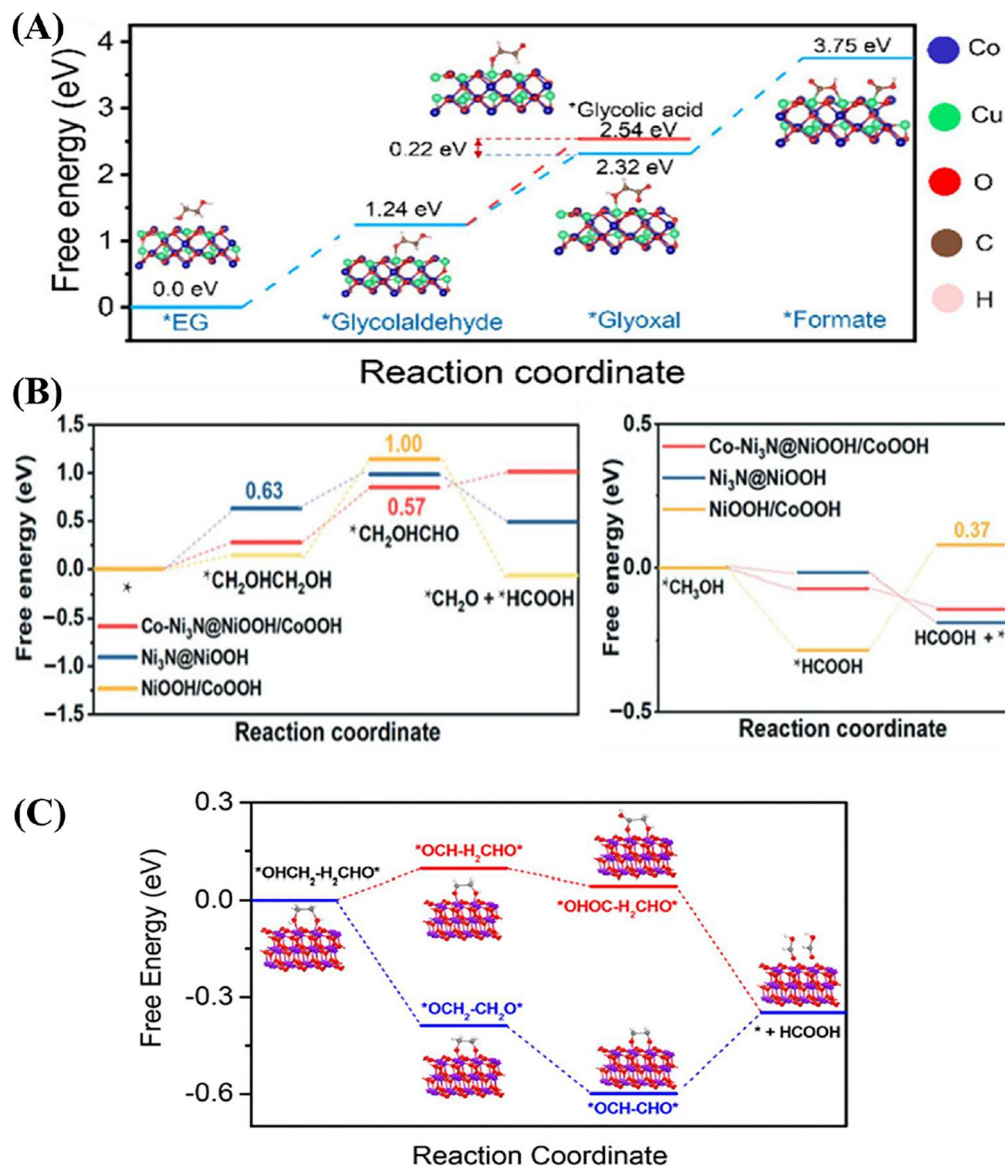


FIGURE 2 Possible C1 pathways indicated by reaction free energy diagrams. (A) Reaction free energy diagram for EGOR on a Co_2CuO_4 catalyst. Reproduced with permission.⁶¹ Copyright 2022, Royal Society of Chemistry. (B) Reaction free energy graph for EGOR on the nitrogen-cobalt nitride nanoflakes. Reproduced with permission.⁹⁰ Copyright 2023, Spring Nature. (C) Free energy schematic for EGOR on CuO. Reproduced with permission.⁹¹ Copyright 2022, American Chemical Society. EGOR, ethylene glycol oxidation reaction.

easy to achieve by the selective oxidation of EG, significant achievements have been achieved in exploring the possible reaction mechanisms of producing C2 products.

For instance, Liu et al.⁵³ revealed the reaction pathway of EG into GA through the density functional theory (DFT) calculations and experiment measurements (Figure 3A). Firstly, $^*\text{HOCH}_2\text{CH}_2\text{OH}$ was formed by the adsorption of EG on the active Pd site of Pd-Ni(OH)₂, followed by the generation of $^*\text{OCH}_2\text{CH}_2\text{OH}$. Afterward, $^*\text{OCH}_2\text{CH}_2\text{OH}$ completed the first dehydrogenation step to yield $^*\text{CHOCH}_2\text{OH}$ with the assistance of $^*\text{OH}$ species, identified from the

activation of OH^- on the Ni site by electron paramagnetic resonance (EPR) experiments. Subsequently, $^*\text{CHOCH}_2\text{OH}$ underwent the second dehydrogenation step to acquire $^*\text{COCH}_2\text{OH}$, the presence of which was proved by the intermediate of 2-hydroxyacetyl ($^*\text{COCH}_2\text{OH}$) through in situ FTIR measurements. Furthermore, $^*\text{COOHCH}_2\text{OH}$ was obtained through the third dehydrogenation. Besides, Du et al.⁹³ revealed pure Pt catalyst presented the same reaction pathway as $^*\text{HOCH}_2\text{CH}_2\text{OH} \rightarrow ^*\text{OCH}_2\text{CH}_2\text{OH} \rightarrow ^*\text{CHOCH}_2\text{OH} \rightarrow ^*\text{COCH}_2\text{OH} \rightarrow ^*\text{COOHCH}_2\text{OH}$ (Figure 3B). However, the Pt/ γ -NiOOH catalyst exhibited a different intermediate of $^*\text{CHOHCH}_2\text{OH}$

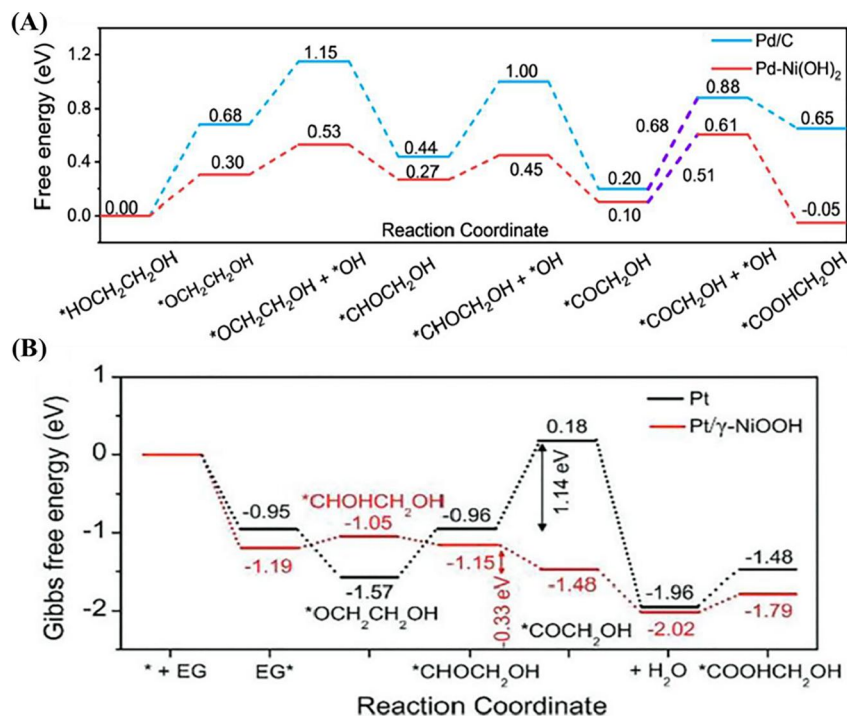


FIGURE 3 Possible C2 pathways indicated by reaction free energy diagrams. (A) EGOR free energy graph on the catalysts of Pd/C and Pd-Ni(OH)₂. Reproduced with permission.⁵³ Copyright 2023, Wiley-VCH GmbH. (B) EGOR free energy graph on the catalysts of Pt and Pt/ γ -NiOOH. Reproduced with permission.⁹³ Copyright 2023, Wiley-VCH GmbH. EGOR, ethylene glycol oxidation reaction.

instead of *OCH₂CH₂OH, which was caused by the synergistic action of Pt and γ -NiOOH.

2.2 | Electrooxidation processes of other plastic waste

PEF stands out as a highly promising biobased alternative to PET, owing to its analogous structure and enhanced CO₂ and oxygen barrier properties when compared to PET.⁹⁴ While PEF is recognized for its biodegradability, it still exhibits a prolonged biodegradation timeline under relevant environmental conditions.⁹⁵ Similar to PET, PEF can undergo hydrolysis under alkaline conditions, resulting in the generation of its constituent monomers, namely 2,5-furandicarboxylic acid (FDCA) and EG (Figure 4A).⁹⁸ Surprisingly, FDCA presents distinct advantages compared to TPA derived from PET hydrolysis. FDCA not only demonstrates a heightened ease of separation from the hydrolyzate of PEF, but this enhanced separability also contributes to improved processability and minimizes potential effects from impurities.⁹⁹ The efficient separation of FDCA allows for its reuse in PEF production, fostering a more sustainable and closed-loop manufacturing process. EG derived from PEF could undergo reaction pathways like that of PET

derived from EG, resulting in the formation of C1 and C2 products.

PBT is known as an engineering thermoplastic endowed with remarkable features. It can be depolymerized through alkaline hydrolysis into the monomers of TPA and 1,4-butanediol (BDO). Subsequently, BDO underwent electrochemical oxidation to produce succinate, as proposed by Liu et al.⁹⁶ The electrochemical reaction pathway for BDO is illustrated in Figure 4B. The process initiated with the formation of 4-hydroxybutanal, leading to two potential pathways. Pathway I involved the initial oxidation of the aldehyde group, resulting in the intermediate 4-hydroxybutanoic acid. Subsequently, the alcohol group underwent oxidation, yielding the desired product of succinic acid. Alternatively, Pathway II involved the oxidation of the alcohol group to produce succinaldehyde as the intermediate. The theoretical analysis strongly suggested that the preferred route for the oxidation of BDO to succinic acid follows Pathway I: BDO \rightarrow OH(CH₂)₃HCO* \rightarrow OH(CH₂)₃-COOH* \rightarrow succinic acid (Green arrow).

Polyamide-66 (PA-66), recognized as nylon 66, ranks among the top five technical plastics with a worldwide demand of 1.3 million tons every year. An integrated approach for the electrochemical

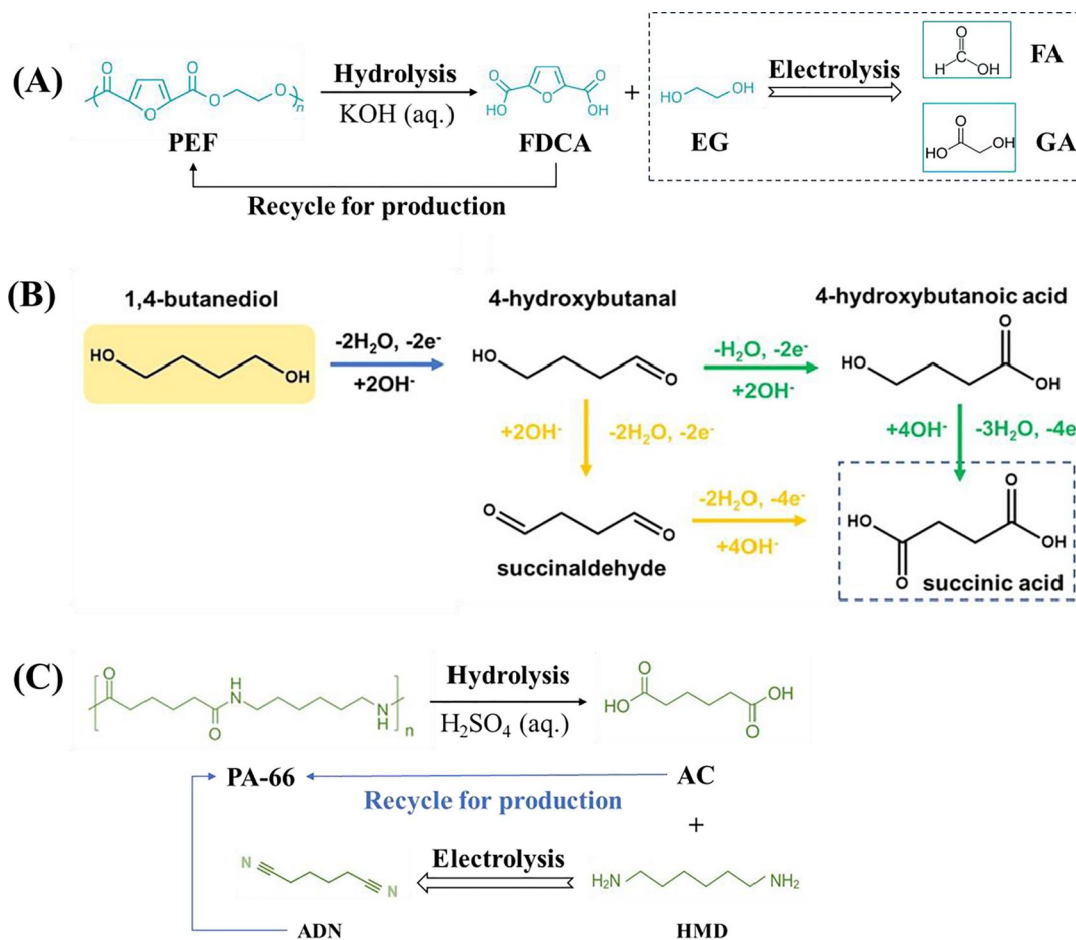


FIGURE 4 Possible conversion pathways of other plastic wastes except PET. (A) Scheme of conversion pathway for PEF. (B) Proposed reaction pathway of BDO oxidation in alkaline media. Reproduced with permission.⁹⁶ Copyright 2023, Elsevier. (C) Scheme of conversion pathway for PA-66. Reproduced with permission.⁹⁷ Copyright 2023, Wiley. AC, adipic acid; ADN, adiponitrile; BDO, 1,4-butanediol; EG, ethylene glycol; FA, formic acid; FDCA, 2,5-furandicarboxylic acid; GA, glycolic acid; HMD, hexamethylenediamine; PA-66, polyamide-6; PEF, polyethylene furanoate; PET, polyethylene terephthalate.

conversion of PA-66 is presented in Figure 4C.⁹⁷ In contrast to PET, the hydrolysis of PA-66 requires implementation under acidic conditions. Under the catalytic hydrolysis of H_2SO_4 , polyamide-66 (PA-66) undergoes conversion into adipic acid (AC) and hexamethylenediamine (HMD). After this reaction, excess acid is efficiently removed through a base treatment process. Following the isolation of AC and HMD, the latter undergoes electrolytic oxidation to yield the valuable adiponitrile (ADN). ADN and AC, derived from end-of-life PA-66, offer the opportunity for sustainable reuse in the production of new PA-66, thus alleviating scarcity concerns of precursors.

PE constitutes a significant portion of plastic waste and is notably one of the most challenging plastics to degrade, with an estimated degradation time of up to 600 years. Similar to PA-66, PE can be broken up under acidic conditions, such as with HNO_3 , resulting in the formation of dicarboxylic acids. Predominantly, the resulting dicarboxylic acids include succinic acid (44%) and glutaric acid

(22%).¹⁰⁰ Subsequently, both succinic acid and glutaric acid have the potential to undergo electrolysis, ultimately producing gaseous products of ethylene and propylene, respectively.

3 | ADVANCED ELECTROCHEMICAL SYSTEMS FOR PLASTIC ELECTRO-REFORMING

To optimize the efficiency of electrical energy utilization throughout the entire electrocatalysis conversion process, it is crucial to integrate plastic electrocatalytic oxidation with suitable cathodic reductions. Furthermore, it is also a moderate and cost-efficient way to produce upgraded chemicals concurrently on both sides through the combination of anode and cathode reactions. Some plastic upcycling-involved co-electrolysis systems have been studied, including HER, CO_2RR , and NO_3RR . Besides, efforts have already been devoted to photo-assisted electrolysis systems.

3.1 | Plastic upcycling integrated with HER

Currently, the oxidation of EG derived from PET waste integrated with HER ($\text{CH}_6\text{O}_2 + \text{OH}^- \rightarrow \text{HCOO}^- + 2\text{H}_2$) could be easily achieved. Besides, the determination of products at the anode could be achieved via various instruments, including NMR, in situ FTIR spectroscopy, HPLC, etc. The collection and detection of H_2 could be realized with the water-gas displacing method and instrument of gas chromatography-mass spectrometry (GC-MS) or GC equipped with a thermal conductivity detector.

The oxidation of EG derived from PET waste integrated with HER could be achieved over noble metal-based or transition metal-based electrocatalysts (Table 1). The co-production of formate and hydrogen could be attained by bifunctional cobalt and nickel-based electrocatalysts, such as phosphides, nitrides, and oxides. Among the studies on Co and Ni phosphides, Zhou et al.⁵⁴ made a remarkable achievement on the EG selective oxidation and the evolution of hydrogen by adopting the bifunctional electrocatalyst of $\text{CoNi}_{0.25}\text{P}/\text{Ni}$ foam (NF). In the test of HER in an alkaline electrolyte, the $\text{CoNi}_{0.25}\text{P}/\text{NF}$ displayed a much higher current density with a low Tafel slope of 58.1 mV dec^{-1} and exhibited a very high current density (350 mA cm^{-2} at 1.7 V vs. RHE) (RHE: reversible hydrogen electrode) toward the EG oxidation in 1 M KOH with 0.3 M EG (Figure 5A). Notably, at a constant potential of 1.7 V versus RHE, the formate Faradaic efficiency (FE) reached 91.7% and the formate generation yield was $4.1 \text{ mmol cm}^{-2} \text{ h}^{-1}$, as well as a long-time stability over 39 h (Figure 5B). A zero-gap membrane-electrode assembly (MEA) flow reactor was designed to test the practicability of the oxidation of EG coupled with the H_2 production (Figure 5C). The considerably higher current density of 500 mA cm^{-2} was obtained through the MEA reactor at a low cell voltage ($<1.8 \text{ V}$), outperforming other phosphide catalysts in Table 1. Besides, the complete upcycling of PET was realized by a sequence of steps including the alkaline hydrolysis, the electrocatalytic oxidation of EG, the PTA, and the syok manthesis of KDF from the formate in the electrolyte. Finally, the products of 818.5 g PTA , 16.9 g H_2 , and 272.4 g KDF were gained (Figure 5D).

It is revealed that hydrogen production efficiency could be affected by the properties of catalysts. For instance, Wang et al.¹⁰⁶ prepared the $\text{CoNi}_{0.2}\text{P-uNS}/\text{NF}$ featuring the ultrathin structure with a high specific area through the cyanogel-hydrolysis approach (Figure 6A). The $\text{CoNi}_{0.2}\text{P-uNS}/\text{NF}$ behaved excellent HER catalytic activity ($\eta_{10} = 43 \text{ mV}$) with a lower Tafel slope of 48.8 mV dec^{-1} than other phosphide catalysts (Figure 6B), which may be ascribed to the arrays constructed from nanosheets in a multi-hierarchical

configuration featuring a substantial active surface area of $\text{CoNi}_{0.2}\text{P-uNS}/\text{NF}$, thus accelerating the mass/charge transport during the HER. Besides, Li et al.¹¹⁰ applied a common two-step approach of hydrolysis and phosphidation to obtain the $\text{Co-Ni}_2\text{P}/\text{NF}$ characterizing with distinct heterointerface structure of CoP and Ni_2P (Figure 6C). Such a heterointerface structure endowed $\text{Co-Ni}_2\text{P}/\text{NF}$ with the overwhelming EGOR catalytic activity ($\eta_{50} = 0.09 \text{ V}$) (Figure 6D) since the electronic structure of Ni and P atoms could be effectively regulated by the unsaturated atomic heterometallic $\text{Co}_x\text{Ni}_{1-x}\text{P}$ sites.

Apart from phosphides, Co or Ni-based nitrides also receive great attention for the electrochemical oxidation of PET waste with the concurrent generation of hydrogen. For example, Liu et al.⁹⁰ fabricated Co-Ni nitride supported on carbon cloth ($\text{Co-Ni}_3\text{N}/\text{CC}$) performed as a bifunctional catalyst (Figure 7A,B). $\text{Co-Ni}_3\text{N}/\text{CC}$ showed an ultra-low overpotential of 81 mV for HER and a low potential of 1.18 V versus RHE for EGOR at the current density of 10 mA cm^{-2} (Figure 7C,D), surpassing other nitride catalysts. The stability evaluation of $\text{Co-Ni}_3\text{N}/\text{CC}$ revealed that only a marginal decline of potential was observed when the operation time reached up to 15 h at the anode (Figure 7E). Additionally, other transition metals such as W and Mo were introduced to modify the Co or Ni-based nitride catalysts. For instance, the bifunctional catalyst of $\text{Ni}_3\text{N-W}_5\text{N}_4$ was obtained through a growth strategy induced by transition metal nitrides (Figure 7F), which efficiently prevented too intense association between N sites and H_{ad} caused by the traditional N-rich synthesis methods.¹⁰⁴ Impressively, a small solar-driven “chemical factory” was established to drive HER and plastic conversion in seawater applying $\text{Ni}_3\text{N}/\text{W}_5\text{N}_4$ as both the cathode and anode (Figure 7G). Notably, such a solar-driven integrated device presented a high current density (156 mA cm^{-2}), corresponding to a solar-to-hydrogen efficiency transformation efficiency of 16.04% under 1 sun illumination.^{111,112}

Transition metal oxides, such as CuCo_2O_4 ⁶¹ and $\text{Mn}_{0.1}\text{Ni}_{0.9}\text{Co}_2\text{O}_{4.8}$,¹⁰⁸ are also active anodes for the electrochemical conversion of EG into C1 products. Nevertheless, noble metals such as Pt are still required to act as the cathode, achieving simultaneous green hydrogen production. It was revealed that the transition metal oxides could not perform as the bifunctional catalysts in the co-electrolysis system of plastic oxidation and hydrogen evolution due to the inability toward HER. In contrast, transition metal-based phosphides and nitrides exhibited better catalytic activity toward EGOR and HER. Compared with transition metal-based phosphides, oxides, and nitrides, transition metal-based sulfides are rarely investigated. Recently, Chen and co-authors proved the huge potential of metal sulfides for the

TABLE 1 Electrochemical activity comparison of EG oxidation integrated with HER.

Electrode (anode//cathode)	Potential for anode (V vs. RHE)	Tafel slope for anode (mV dec ⁻¹)	Overpotential for cathode (mV)	Tafel slope for cathode (mV dec ⁻¹)	Cell voltage (V)	FE (oxidation products)	Products	Ref.
CuCo ₂ O ₄ NWA/NF//Pt/NF	$E_{10} = 1.23$	–	–	–	1.56 at 100 mA cm ⁻²	93.0%	H ₂ + formate	61
B,Co–NiS//B,Co–NiS	$E_{100} = 1.341$	32	$\eta_{10} = 86$	81	1.491 at 100 mA cm ⁻²	93.0%	H ₂ + formate	101
CuO nanowires	$E_{10} = 1.38$	96	–	–	–	88.0%	H ₂ + formate	91
Pd–NiTe/NF//Pd–NiTe/NF	$E_{10} = 0.019$	84.5	–	–	1.6 at 10 mA cm ⁻²	95.6%	H ₂ + formate	102
Ni(OH) ₂ /NF//Ni(OH) ₂ /NF	$E_{100} = 1.31$	–	–	–	1.52 at 100 mA cm ⁻²	93.2%	H ₂ + formate	103
NiN ₃ –W ₅ N ₄ //NiN ₃ –W ₅ N ₄	$E_{10} = 1.33$	–	–	34	1.4 at 10 mA cm ⁻²	85.0%	H ₂ + formate	104
OMS–Ni1–CoP	$E_{10} = 1.3$	108.2	$\eta_{10} = 119$	74.6	1.52 at 10 mA cm ⁻²	96.0%	H ₂ + formate	105
Co–Ni ₃ N/CC//Co–Ni ₃ N/CC	$E_{10} = 1.18$	78	$\eta_{10} = 81$	74.1	1.46 at 50 mA cm ⁻²	92.0%	H ₂ + formate	90
CoNi _{0.2} P–uNS/NF//CoNi _{0.2} P–uNS/NF	$E_{10} = 1.3$	39.9	$\eta_{10} = 43$	48.8	1.24 at 50 mA cm ⁻²	92.0%	H ₂ + formate	106
N–Ni ₃ P–NiMoO ₄ /NF//N–Ni ₃ P–NiMoO ₄ /NF	$E_{100} = 1.33$	20.8	$\eta_{100} = 142$	98.5	1.6 at 100 mA cm ⁻²	92.2%	H ₂ + formate	107
CoNi _{0.25} P/NF//CoNi _{0.25} P/NF	$E_{350} = 1.7$	–	$\eta_{10} = 89.9$	58.1	<1.8 at 500 mA cm ⁻²	91.7%	H ₂ + formate	54
Mn _{0.1} Ni _{0.9} Co ₂ O ₄₋₈ //Pt	$E_{50} = 1.42$	–	–	–	–	95.0%	H ₂ + formate	108
Pd/NF//NF	$E_{400} = 0.7$	–	–	–	1.01 at 100 mA cm ⁻²	93.0%	H ₂ + formate	109
Co–Ni ₂ P/NF//Co–Ni ₂ P/NF	$E_{50} = 0.09$	–	$\eta_{10} = 69$	128	1.43 at 10 mA cm ⁻²	–	H ₂ + formate	110
Pt/ γ -NiOOH/NF//Pt/ γ -NiOOH/NF	$E_{450} = 0.79$	–	$\eta_{100} = 86$	17.9	0.8 at 130 mA cm ⁻²	>90%	H ₂ + glycolate	93
Au/Ni(OH) ₂ /NF//NF	$E_{326.2} = 1.15$	–	–	–	1.4 at 4.7 A	91.0%	H ₂ + glycolate	68
Pd/Ni(OH) ₂ /NF//Ni ₂ P/NF	$E_{600} = 1.15$	189	–	–	1.2 at 100 mA cm ⁻²	–	H ₂ + glycolate	53

Note: Some values of overpotential for anode/cathode are cautiously read from the figures in their publication.

Abbreviations: EG, ethylene glycol; FE, Faradaic efficiency; HER, hydrogen evolution reaction; NF, Ni foam; OMS, organized macroporous superstructure; Ref., reference; RHE, reversible hydrogen electrode; uNS, ultra-thin nanosheets.

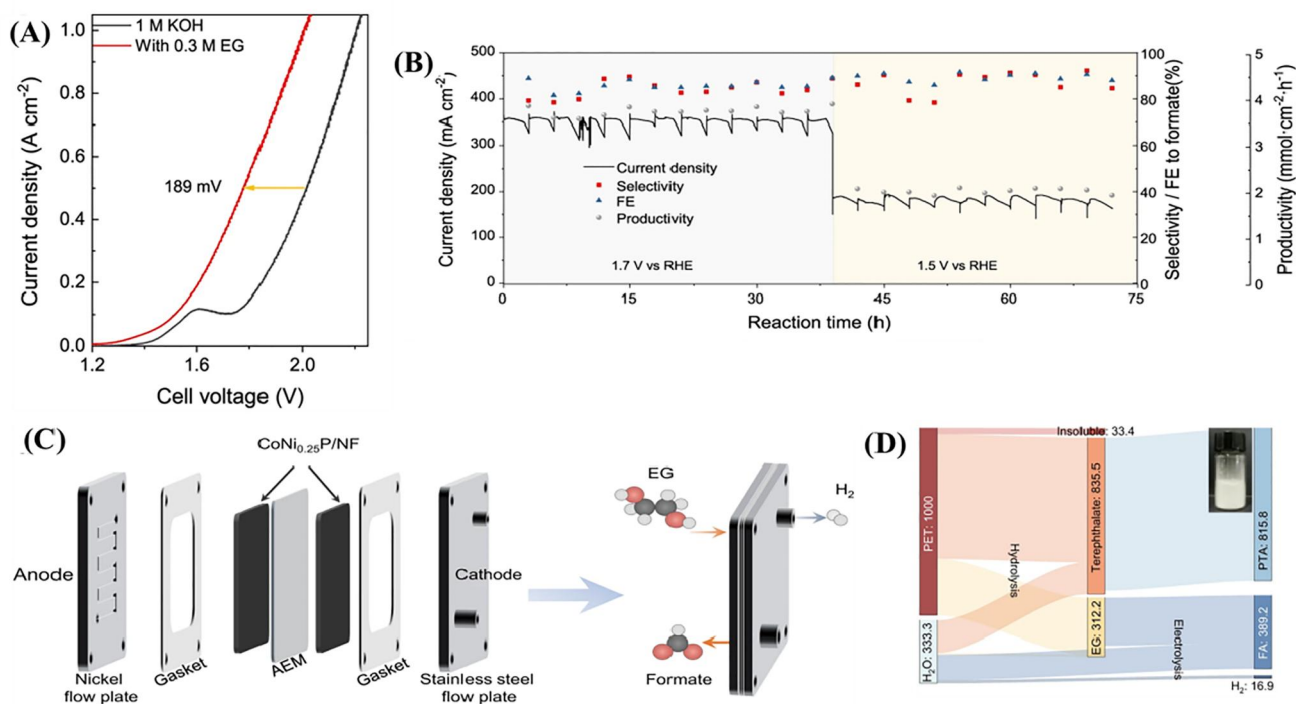


FIGURE 5 Electrochemical catalytic performances of representative bifunctional catalysts of CoNi_{0.25}P/NF. (A) Polarization curves for water splitting and EG electrolysis in the MEA flow reactor. (B) Chronoamperometric stability test for EG oxidation at 1.7 V versus RHE for 13 cycles and 1.5 V versus RHE for 11 cycles. The electrolyte was refreshed every 3 h. (C) The MEA setup for paired HER (-)/EG oxidation (+). (D) Sankey graph illustrating the substance transfer of PET upgrading, with an inset image showing the isolated high-purity PTA. Reproduced with permission.⁵⁴ Copyright 2021, Spring Nature. AEM, anion exchange membrane; EG, ethylene glycol; FA, formic acid; FE, Faradaic efficiency; HER, hydrogen evolution reaction; MEA, membrane-electrode assembly; PET, polyethylene terephthalate; PTA, terephthalic acid; RHE, reversible hydrogen electrode.

electrocatalytic conversion of EG in parallel with the production of hydrogen.¹⁰¹ The potential of 1.341 V versus RHE was required at the current density of 100 mA cm⁻² for EGOR over B and Co co-doped NiS.

Besides, noble metal-involved catalysts, such as Pd-NiTe/NF¹⁰² and Pd/NF,¹⁰⁹ inevitably exhibited higher EG oxidation activity than transitional metal-based catalysts. It was reported that noble metal (e.g., Pd, Pt, Au) based catalysts could enhance the selectivity of EG oxidation to C2 products with a relatively high yield of hydrogen. For example, Pd/Ni(OH)₂ supported on Ni foam served as the anode to selectively convert EG derived from PET waste (Figure 8A), obtaining high industrial current densities of 600 mA cm⁻² at a moderate potential of 1.15 V versus RHE (Figure 8B).⁵³ Although Pd-based catalysts behaved with excellent catalytic performance toward the EG oxidation, some disadvantages still existed such as large operation voltage (>1 V) and significant noble metal loading (>1 mg cm⁻²). In light of this, γ -NiOOH nanosheets attached with Pt nanoparticles on Ni foam (Pt/ γ -NiOOH/NF) was developed by Du et al.⁹³ for the electrochemical conversion of EG into glycolate (Figure 8C). Under a marginal applied voltage of 0.8 V, a FE of 90% and a high

current density of 130 mA cm⁻² could be reached (Figure 8D), achieving small electricity input. Furthermore, the loading amount of Pt of 0.18 mg cm⁻² was far below that of Pd (1.5 mg cm⁻²), realizing the minor utilization of noble metals.

In addition to PET plastic, other plastics, such as PEF, PLA, PE, PA-66, and PMMA, also have been investigated for plastic electro-reforming-assisted green hydrogen production. Ren et al.⁹⁸ applied a NiCo₂O₄ electrocatalyst for the concurrent production of FA and hydrogen with a high FE of 98% toward formate (Figure 9A). The electrocatalytic oxidation of PLA could also be realized via Co-based catalysts. For example, Li et al.¹¹³ prepared 0.1-CoSe₂/NF as a bifunctional catalyst for the simultaneous PLA oxidation and HER. An overpotential of 116 mV (η_{10}) for HER was demanded with a small Tafel slope of 94.4 mV dec⁻¹ and about 150 mV versus RHE for the PLA oxidation reaction was required to reach a current density of 50 mA cm⁻². The electrooxidation products of PLA were determined to be acetic acid by the GC-flame ionization detection instrument, implying the successful conversion of PLA to valuable chemicals (Figure 9B). Xiao et al.⁹⁷ reported the electrochemical upcycling of PA-66, coupled with the

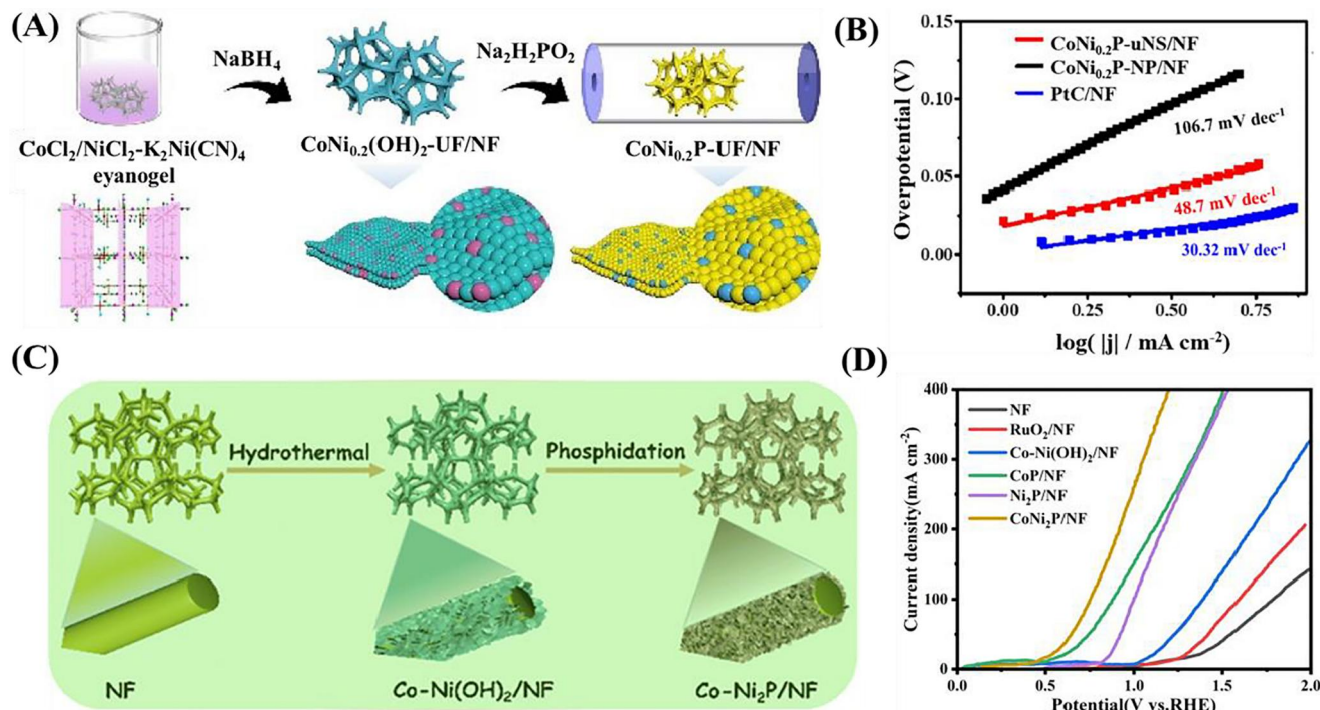


FIGURE 6 Synthesis schemes and electrochemical catalytic performances of representative bifunctional Co and Ni phosphide catalysts. (A) Synthetic procedures of $\text{CoNi}_{0.2}\text{P-uNS/NF}$ hybrids. (B) Tafel slopes of HER at $\text{CoNi}_{0.2}\text{P-uNS/NF}$, $\text{CoNi}_{0.2}\text{P-NP/NF}$, and PtC/NF in 1 M KOH solution at 5 mV s^{-1} . Reproduced with permission.¹⁰⁶ Copyright 2023, Elsevier. (C) Schematic of the synthetic method of $\text{Co-Ni}_2\text{P/NF}$. (D) LSV curves of $\text{Co-Ni}_2\text{P/NF}$, $\text{Ni}_2\text{P/NF}$, CoP/NF , $\text{Co-Ni(OH)}_2/\text{NF}$, RuO_2/NF , and NF anodes in the electrolyte of 1 M NaOH with 5 g L^{-1} PET. Reproduced with permission.¹¹⁰ Copyright 2022, Royal Society of Chemistry. HER, hydrogen evolution reaction; LSV, linear sweep voltammetry; NF, Ni foam; PET, polyethylene terephthalate.

HER. The pivotal phase involving the selective dehydrogenation of C–N bonds within HMD to nitrile $\text{C}\equiv\text{N}$ bonds was successfully achieved using the $\text{Ni}_3\text{S}_2@\text{Fe}_2\text{O}_3$ core-shell catalyst (Figure 9C). This process yielded AND with a nearly perfect FE at 1.40 V, as demonstrated during a 100-h stability test, even under a current density of 100 mA cm^{-2} . Pichler et al.¹⁰⁰ investigated the electrocatalytic process of PE coupling with HER using succinic acid and decomposed PE as the respective substrates (Figure 9D). The findings revealed that under methanolic conditions, the oxidation reaction of succinic acid exhibited a Faradaic yield for ethylene of 38%. However, when the substrate was substituted with decomposed PE, the Faradaic yields for ethylene significantly decreased, indicating a hindrance to the presence of mixed intermediates in the electrochemical process.

The up-cycling of PE could also be achieved by the pathway of manganese-electrocatalysis, yielding the $\text{C}(\text{sp}^3)\text{-H}$ azidated materials (Figure 9E).¹¹⁴ Given the insolubility of PMMA in the water, the model molecule of methyl pivalate (MP) with a similar functional group as PMMA was selected to investigate the potential of electrochemical valorization of PMMA particles under the low temperature.¹¹⁵ Using a proton exchange membrane reactor with Nafion® protonic

membranes and Pt/C electrodes at low temperatures ($<90^\circ\text{C}$) (Figure 9F), the conducted experiments have illustrated that the electrochemical conversion of MP enables the production of H_2 within an electrical potential range where water electrolysis is thermodynamically impractical ($<1.2 \text{ V}$). Furthermore, to tackle the issue of PMMA insolubility, an isopropanol/ H_2O binary solvent was introduced in a liquid batch electrochemical cell, achieving concurrent hydrogen generation and PMMA upgrading.¹¹⁶

3.2 | Plastic up-cycling integrated with NO_3^- RR

The disposal of nitrate has attracted great attention of the public due to its trigger for water eutrophication.¹¹⁷ The electrocatalytic reduction technology could not only solve the problem of nitrate pollution but also convert nitrate into value-added ammonia or N_2 , a critical commodity chemical and carbon-free energy carriers.^{117–119} Therefore, it is promising to integrate nitrate reduction with plastic oxidation in the electrochemical process.^{118,120,121} Overall, in contrast with widely studied HER, NO_3^- RR coupled with plastic oxidation has been less explored.

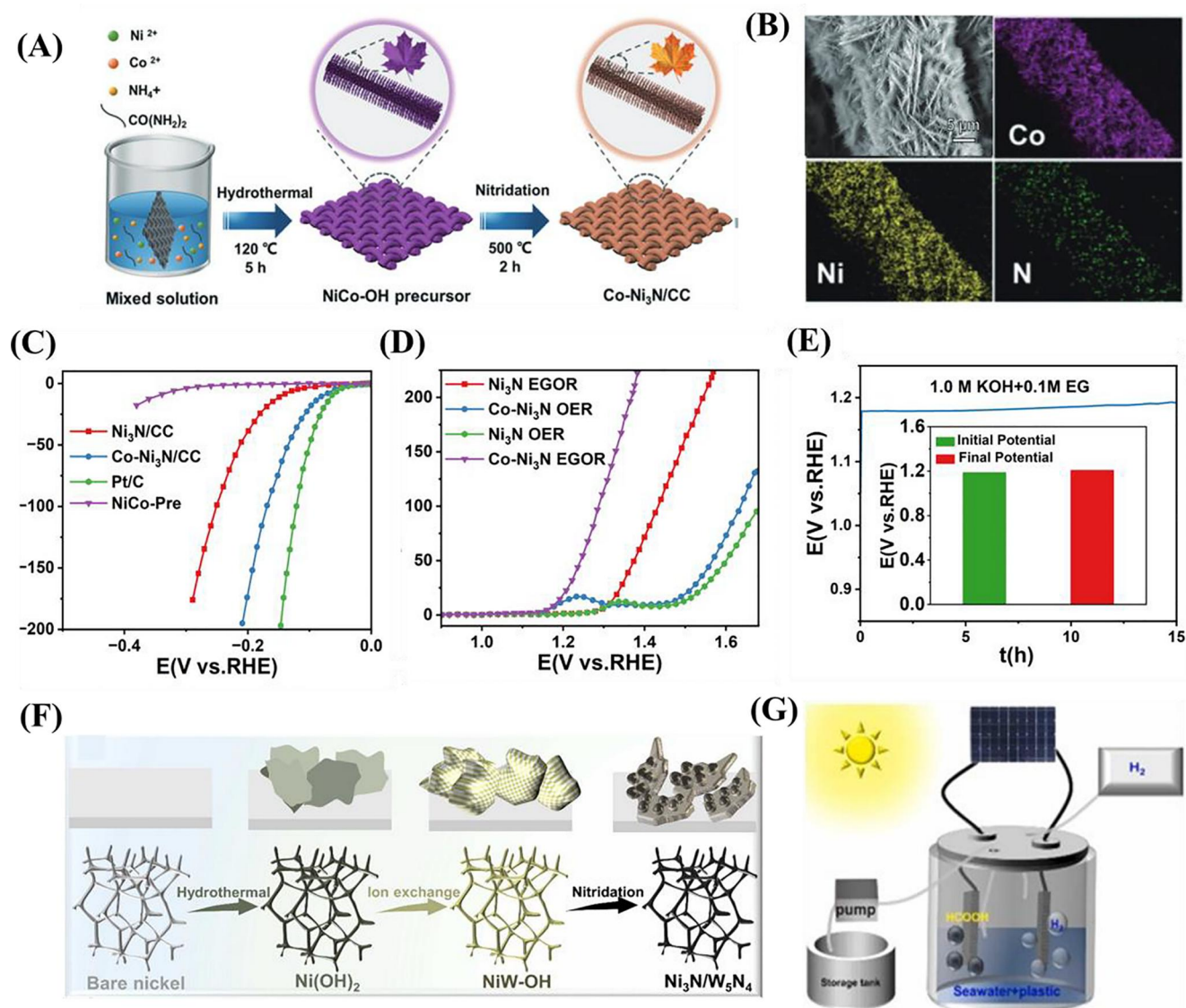


FIGURE 7 Synthesis schemes, characterizations, and electrochemical catalytic performances of representative Co and Ni nitride catalysts. (A) Schematic illustration of the synthesis of the Co-Ni₃N/CC electrode. (B) SEM-EDX element mapping images of Co, Ni, and N elements in Co-Ni₃N/CC electrode. (C) LSV curves for HER in 1.0 M KOH. (D) LSV curves for Co-Ni₃N/CC and Ni₃N/CC in 1.0 M KOH with and without the addition of 0.1 M EG. (E) Chronopotentiometry curves of EGOR at Co-Ni₃N/C. (F) Schematic illustration of constructing the Ni₃N/W₅N₄ electrode with Janus nanostructures. (G) Schematic illustration of a small factory powered by solar energy for HER and plastics upgrading. Reproduced with permission.¹⁰⁴ Copyright 2022, Elsevier. EDX, energy-dispersive X-ray; EG, ethylene glycol; EGOR, ethylene glycol oxidation reaction; HER, hydrogen evolution reaction; LSV, linear sweep voltammetry; RHE, reversible hydrogen electrode; SEM, scanning electron microscope.

A recent study by Ren et al.⁶⁹ could provide some guidelines for the investigation of this integrated system. Firstly, the conversion of PET waste into the C1 product coupled with the generation of ammonia was realized by a functional pre-catalyst of Co-based metal-organic frameworks, which was then transformed into Ru-Co(OH)₂ at the cathode and Ru-CoOOH at the anode, respectively (Figure 10A). The cathodic nitrate reduction was performed in 1 M KOH containing 200 ppm KNO₃, displaying

higher catalytic activity than HER. At a potential of -0.3 V versus RHE, the best catalytic performance was observed, with the NH₃ yield rate of 0.244 mmol h⁻¹ cm⁻² and NH₃ FE of 94.3% (Figure 10B). The concentration-time curves for 2 h revealed that the concentration of NO₃-N gradually decreased, and the concentration of NH₃-N slowly increased while almost no NO₂-N was observed, implying the high selectivity of Ru-Co(OH)₂. Meanwhile, the linear sweep voltammetry (LSV) curves

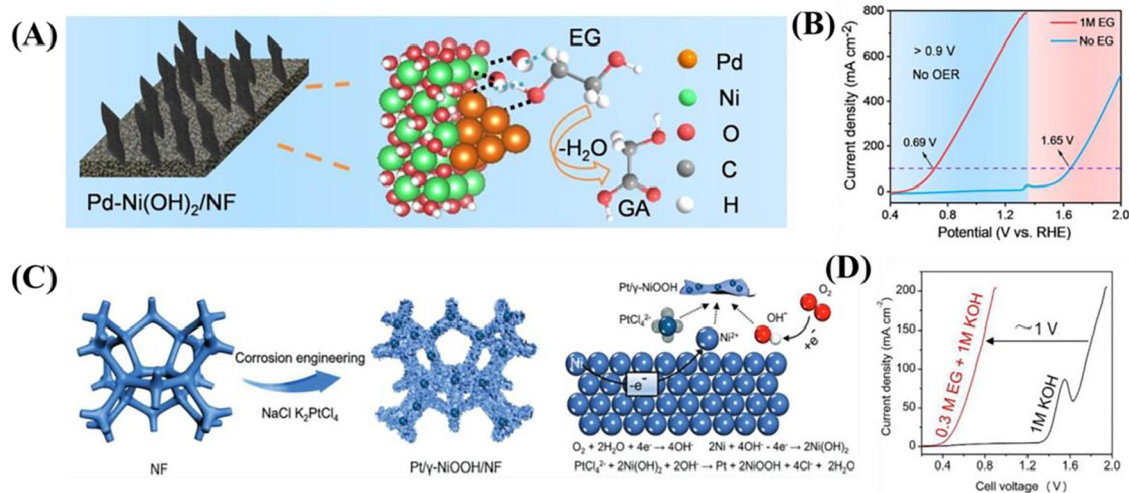


FIGURE 8 Synthesis schemes and electrochemical catalytic performances of representative noble metal supported on nickel foam catalysts. (A) Diagrammatic depiction of the Pd Ni(OH)₂ fabrication on Ni foam. (B) Polarization curves for Pd Ni(OH)₂/NF in 1.0 M KOH, both in the presence and absence of ethylene glycol. Reproduced with permission.⁵³ Copyright 2023, Wiley-VCH GmbH. (C) Schematic illustration of Pt/γ-NiOOH/NF preparation using corrosion engineering. (D) Polarization curves for overall water splitting and electro-reforming of PET hydrolyzate at a scan rate of 5 mV s⁻¹. Reproduced with permission.⁹³ Copyright 2023, Wiley-VCH GmbH. EG, ethylene glycol; GA, glycolic acid; NF, Ni foam; OER, oxygen evolution reaction; PET, polyethylene terephthalate; RHE, reversible hydrogen electrode.

revealed that a lower potential for EG oxidation was required than that for OER at a current density of 100 mA cm⁻². At an applied potential of 1.33 V versus RHE, the FE of the main product of formate (at the anode) reached 96.53%, which exhibited better oxidation performances of PET hydrolyzates (Figure 10C). After six consecutive cycles, the formate remained stable, verifying the excellent stability of the anodic catalyst (Figure 10D). The performance of the integrated system ((-) NO₃⁻RR// PET hydrolyzate oxidation (+)) was evaluated in an H-type cell with a two-electrode system. At a voltage of 2.3 V versus RHE, a formate FE of 97.93%, an NH₃ FE of 96.43% and an NH₃ yield rate of 0.222 mmol h⁻¹ cm⁻² were obtained (Figure 10E).

On the other hand, the integration of PET hydrolyzate oxidation into C2 products and the nitrite reduction was achieved using low-crystalline CoOOH (LC-CoOOH/CF) and Pd nanothorns (Pd NTs/NF) as cathode and anode, respectively (Figure 10F).¹²² At the potential of -0.25 V versus RHE, NO₃⁻ was completely converted into NH₃, achieving the maximum NH₃ FE (97.38 ± 1.0%). It was observed that the obvious oxidation of EG derived from PET hydrolyzate occurred at the potential range of 0.6–1.6 V versus RHE. Furthermore, the selectivity of Pd NTs/NF toward C2 products showed the highest value at a lower potential of 0.774 V versus RHE. The coupling generation system of NH₃ and GA displayed the maximum FE of GA (90.12 ± 3.6)% and NH₃ (94.47 ± 2.8)% at 1.0 and 1.2 V, respectively (Figure 10G).

3.3 | Plastic up-cycling integrated with CO₂RR

The excessive emission of CO₂ aggravates global warming, thereby causing sequent environmental problems such as water resource crises and extreme climate.¹²³ Therefore, the utilization of CO₂ becomes a promising way to relieve environmental and energy issues. Notably, electrocatalysis has been demonstrated to be efficient in converting CO₂ into high-valued chemicals and fuels.^{124–126} Based on the electro-reforming of plastic waste, the integrated valorization of CO₂ and plastic waste seems to be a prospective strategy, which involves the cathodic CO₂ reaction and anodic oxidation reaction of plastic waste simultaneously.

Take the research of Li et al.⁵⁵ as an example, a two-electrode (anode: NiCo₂O₄/CFP, cathode: SnO₂/CC) electrolyzer was constructed to evaluate the performance of the integrated system to coproduce the FA (Figure 11A). With regards to the electrocatalytic oxidation of PET hydrolyzate, the FE of FA was determined to be stable at least 90% with different charges passed. The oxidation product of FA was identified by the ¹³C NMR and ¹H NMR analysis, corresponding to the peak at 165.7 ppm and the peak at 8.3 ppm, respectively (Figure 11B). As for the CO₂ reduction reaction, the selectivity of SnO₂/CC electrocatalyst toward FA was sensitive to the applied potential and the maximum FA FE of (82 ± 2)% reached at an applied potential of -0.9 V versus RHE, with the least amount of H₂ and CO (Figure 11C). The

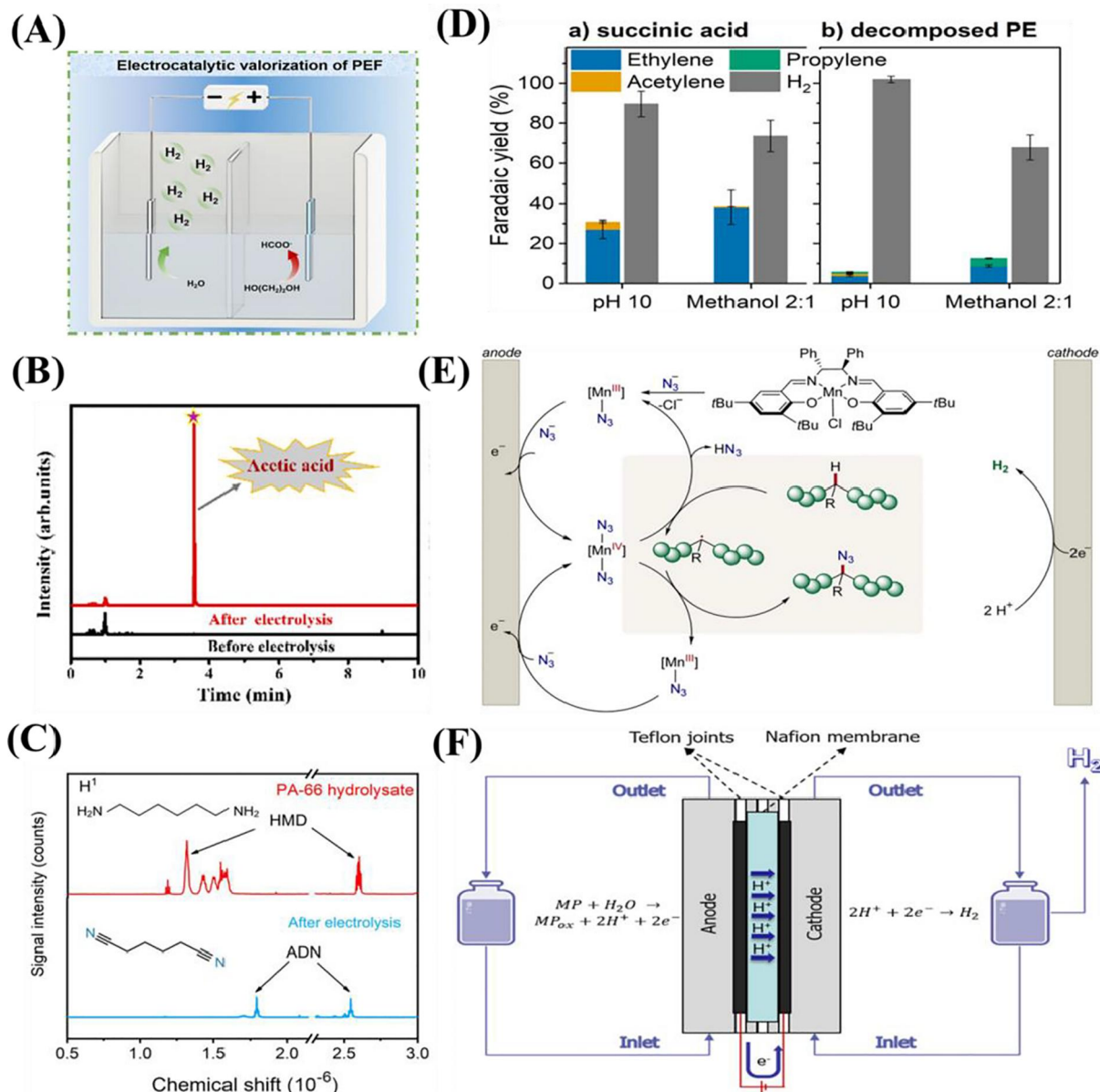


FIGURE 9 Electrochemical catalytic performances for the oxidation of other plastic wastes. (A) Electrocatalytic valorization of PEF hydrolysate for formate and hydrogen energy production. Reproduced with permission.⁹⁸ Copyright 2016, Royal Society of Chemistry. (B) GC-FID quantification of the collected PLA electrooxidation products. Reproduced with permission.¹¹³ Copyright 2022, Royal Society of Chemistry. (C) ^1H NMR spectra of PA-66 hydrolysate and anolyte. Reproduced with permission.⁹⁷ Copyright 2023, Wiley. (D) Electrolysis results of succinic acid solution and PE decomposition solution. Reproduced with permission.¹⁰⁰ Copyright 2021, American Chemical Society. (E) Proposed mechanism for manganese-catalyzed C-H azidation of commodity polymers. Reproduced with permission.¹¹⁴ Copyright 2023, Royal Society of Chemistry. (F) Scheme of the PEM-based experimental set-up.¹¹⁵ Copyright 2020, Elsevier. ADN, adiponitrile; GC-FID, gas chromatography-flame ionization detection; HMD, hexamethylenediamine; NMR, nuclear magnetic resonance; PA-66, polyamide-66; PE, polyethylene; PEF, polyethylene furanoate; PEM, proton exchange membrane; PLA, polylactic acid.

stability evaluation test revealed that after 12 h of continuous electrolysis, no slight decrease in the catalyst activity for FA production from CO_2 reduction was observed. In contrast with the typical system of OER coupled with CO_2RR , the replacement of OER with PET oxidation led to a decrease by 1.55 V of the onset-driven voltage and an obvious increase in the current density. The FA production ability of the total

integrated system was examined, and a high FE of about 155% for FA at 1.9 V was achieved, verifying the excellent performance of the concurrent FA production system.

Nanocomposites that combine oxides with carbon supports have emerged as promising materials for enhancing the plastic electrochemical oxidation process coupled with CO_2RR . Notably, two specific

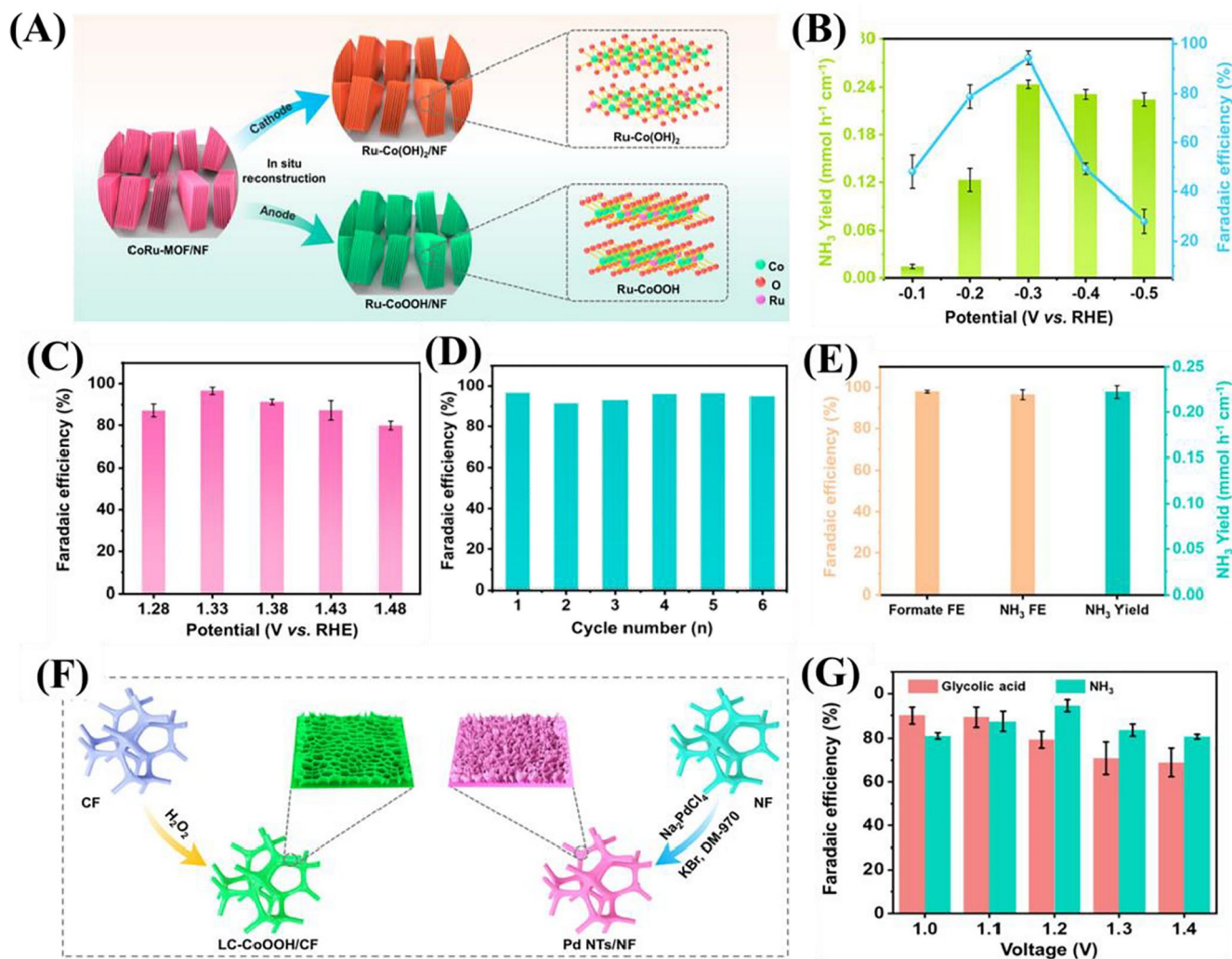


FIGURE 10 Synthesis schemes and electrochemical catalytic performances of representative catalysts for NO₃⁻RR. (A) Synthetic scheme of Ru-Co(OH)₂/NF and Ru-CoOOH/NF. (B) NH₃ yield rates and NH₃ Faradaic efficiency over Ru-Co(OH)₂/NF at various potentials. (C) Faradaic efficiency of PET hydrolyzate oxidation to formate with various potentials. (D) Faradaic efficiency of PET hydrolyzate oxidation to formate of Ru-CoOOH/NF for consecutive cycles at 1.33 V versus RHE. (E) Formate Faradaic efficiency, NH₃ Faradaic efficiency and yield rates over the CoRu-MOF/NF precatalyst at 2.3 V (without iR compensation). Reproduced with permission.⁶⁹ Copyright 2023, American Chemical Society. (F) Schematic illustration of LC-CoOOH/CF and Pd NTs/NF. (G) Faradaic efficiency of NH₃ and GA with various voltages. Reproduced with permission.¹²² Copyright 2023, American Chemical Society. CF, carbon fiber; DM-970, (C₂H₄O)_n-C₂₄H₄₂O-C₁₅H₂₄O; GA, glycolic acid; LC, low-crystalline; MOF, metal-organic frameworks; NF, Ni foam; NO₃⁻RR, NO₃⁻ reduction reaction; NTs, nanothorns; PET, polyethylene terephthalate; RHE, reversible hydrogen electrode.

catalysts, bismuth oxide carbonate (BOC) supported on reduced graphene oxide (rGO) and CuCoO strained on rGO (CuCoO@rGO), have been investigated for their efficacy in cathodic CO₂RR and anodic PET hydrolyzate oxidation, respectively, to simultaneously produce formate (Figure 11D).¹²⁷ The anodic CuCoO@rGO catalyst has demonstrated exceptional electro-activity, achieving a remarkable FE of 85.7% at 1.5 V versus RHE. On the other hand, the cathodic BOC@rGO catalyst exhibited an impressive FE of 97.4% at -0.8 V versus RHE, expediting efficient formate production from CO₂RR. The utilization of these catalysts in an electrolyzer has enabled the generation of FA at a low cell voltage of 1.9 V at

10 mA cm⁻², with the formate FE reaching 151.8% (Figure 11E).

3.4 | Photoelectrochemical systems

PEC technology, a combination of photocatalytic and electrocatalytic technologies, could efficiently utilize the photovoltage effect, thus decreasing the external bias and electricity input.^{128,129} Like pure electrolytic technology, the integration of anodic oxidation and cathodic reduction to produce high-valued chemicals via the photoelectron pathway has also been explored. As a main targeted plastic waste, PET

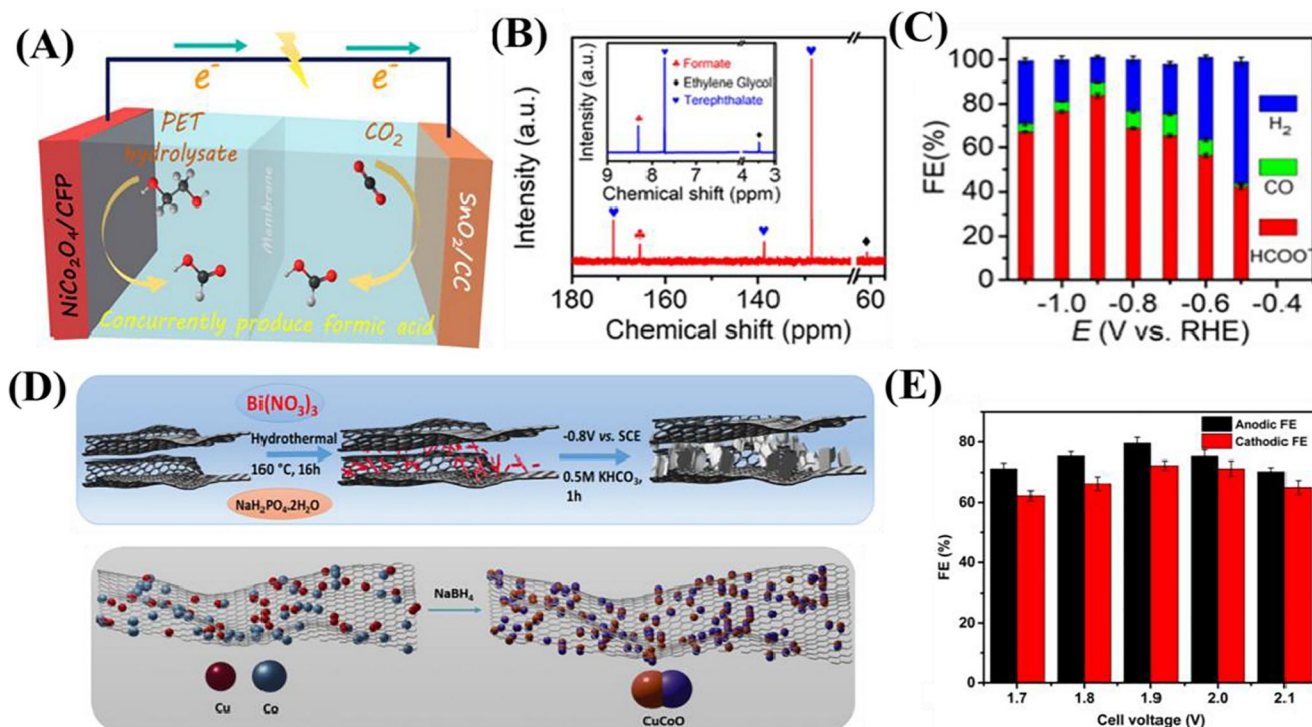


FIGURE 11 Synthesis schemes and electrochemical catalytic performances of representative catalysts for CO₂RR. (A) Concurrent electrochemical conversion of anodic PET hydrolyzate and cathodic CO₂ to formic acid. (B) 3C NMR and 1H NMR (inset) spectra of the electrolyte with PET hydrolyzate after electrolysis. (C) Faradaic efficiencies of the SnO₂/CC electrode for the CO₂RR at different potentials. Reproduced with permission.⁵⁵ Copyright 2022, American Chemical Society. (D) Synthetic scheme BOC@rGO and CuCoO@rGO. (E) Faradaic efficiencies at both cathode and anode at each potential employing the 2-electrode integrated electrolyzer. Reproduced with permission.¹²⁷ Copyright 2023, The Royal Society of Chemistry. CC, carbon cloth; CFP, carbon fiber paper; CO₂RR, CO₂ reduction reaction; FE, Faradaic efficiency; NMR, nuclear magnetic resonance; PET, polyethylene terephthalate; SCE, saturated calomel electrode.

oxidation occurring at the anode has been coupled with several reduction processes, such as the biosynthetic reaction,¹³⁰ CO₂RR,¹³¹ and HER.^{132–134} In the PEC system, the PEC conversion efficiency largely depends on the photoelectrode materials composed of light-harvesting semiconductor adsorbers and the electrode reaction-triggered cocatalysts.¹³⁵ Therefore, it is of great significance to develop photoelectrode materials with the merits of high selectivity, reactivity, and durability.

Fe₂O₃ semiconductor is proved as an ideal candidate for the rational design of photoanode materials, combining with transition metal hydroxides or phosphates cocatalysts such as Ni(OH)_x and Ni-Pi.^{132,133} For instance, Li et al.¹³² fabricated a photoanode of Fe₂O₃/Ni(OH)_x using a facile hydrothermal strategy for PET hydrolyzate oxidation (Figure 12A). Notably, the Ni amount of *x* could determine the ratio of Ni²⁺ and Ni³⁺, thus realizing the regulation of the oxidation ability of photogenerated holes to PET through the involvement of Ni²⁺/Ni³⁺ redox couple.¹³² Finally, Fe₂O₃-10Ni exhibited better reactivity and high selectivity toward the conversion of PET into FA, identified by ¹H NMR spectra (Figure 12B). To further enhance the catalytic performance of Fe₂O₃-based photoanode

materials, transition metals such as Zr and Ti have also been introduced to modify the structure and property of photoanode to boost its intrinsic catalytic activity.^{130,136}

Lead halide perovskites are commonly employed as the light adsorbers of photocathodes, integrating with the cathodic catalysts to complete some reduction reactions including CO₂RR and HER.^{131,134} For example, hydrogen generation in parallel with the upcycling of plastic waste was achieved using a Cu₃₀Pd₇₀/perovskite/Pt PEC device.¹³⁴ To determine the performance of the PEC device, two-compartment and “artificial leaf” configurations were designed as shown in Figure 12C,D. The model substrate EG oxidation coupling HER was conducted in 1 M KOH solution in the two-compartment configuration. (1316 ± 269) μmol H₂ cm⁻² was generated after an operation period of 10 h. Meanwhile, the yield and selectivity of GA were acquired to be (163 ± 45) μmol and (95 ± 2)%, respectively. The eligibility of real-world plastic waste for this system was verified in the integrated Cu₃₀Pd₇₀|perovskite|Pt “artificial leaf.” Experiment results showed that the photocurrent density of (5.2 ± 0.4) and (4.7 ± 0.3) mA cm⁻² was gained from PET powder and

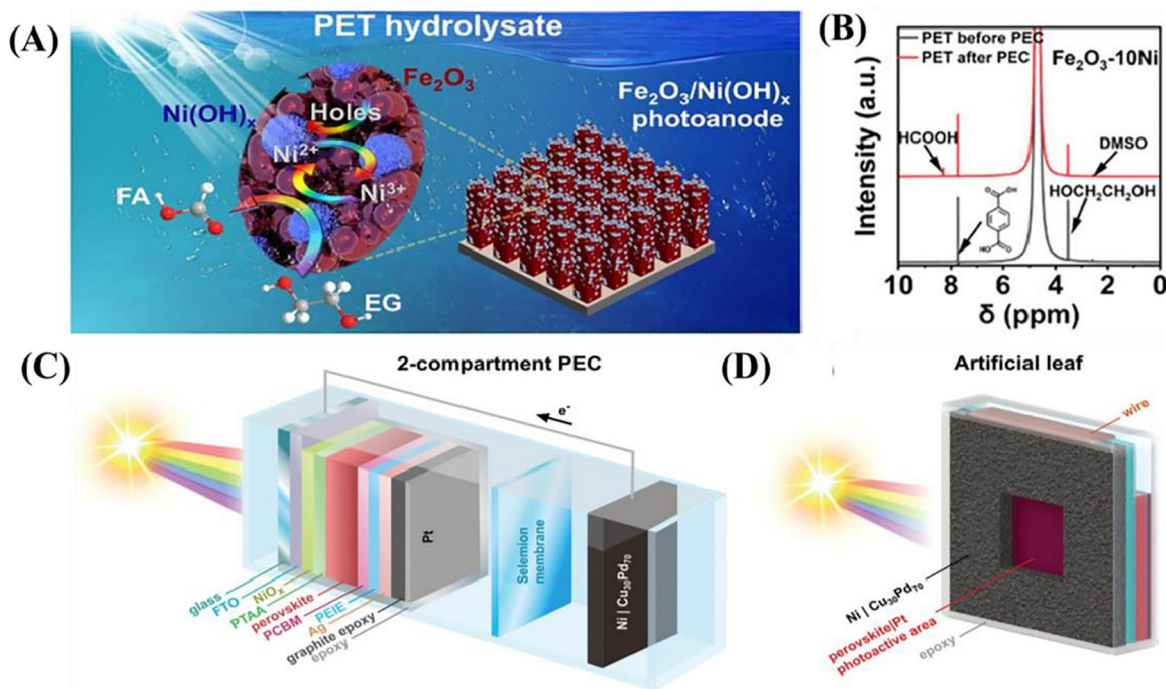


FIGURE 12 Photoelectrochemical catalytic performances of representative catalysts and representative photoelectrochemical catalytic setups for PET oxidation. (A) Scheme of PEC catalysis of PET plastic waste. (B) Results of ^1H NMR of the oxidation products via PEC valorization of the PET hydrolyzate by $\text{Fe}_2\text{O}_3\text{-10Ni}$ at 1.2 V versus RHE. Reproduced with permission.¹³² Copyright 2022, American Chemical Society. Schematic depictions of the $\text{Cu}_{30}\text{Pd}_{70}$ |perovskite|Pt system in (C) two-compartment, and (D) standalone “artificial leaf” configurations. Reproduced with permission.¹³⁴ Copyright 2022, Wiley-VCH GmbH. DMSO, dimethyl sulfoxide; EG, ethylene glycol; FA, formic acid; NMR, nuclear magnetic resonance; PEC, photoelectrochemical; PET, polyethylene terephthalate; RHE, reversible hydrogen electrode.

bottle hydrolyzate oxidation respectively, lower than that from the EG model molecule. Besides, the H_2 amounts generated from hydrolyzed PET powder and bottle were 776 and 748 $\mu\text{mol cm}^{-2}$ respectively, much lower than that from pure EG. It was suggested that the presence of terephthalate inhibited EG oxidation. Nevertheless, the yield and selectivity of GA from the pretreated PET polymers retained insignificant differences compared with the model molecule of EG.

4 | ELECTROCATALYST DESIGN STRATEGIES

Currently, the exploration of highly efficient electrocatalysts for plastic electro-reforming has received huge attention.¹³⁷ For example, transition metal-based catalysts, including oxides, phosphides, and nitrides, have been well investigated for the electrocatalytic conversion of PET into C1 products. Additionally, nickel hydroxide-supported noble metal electrocatalysts have exhibited excellent catalytic activity toward the transformation of PET into C2 products. We summarize representative electrocatalysts for electrooxidation of plastic waste in Table 2.

To optimize the catalytic performance, strategies have been developed to improve the effectiveness, selectivity, and stability of electrocatalysts.¹³⁹ The main modification engineering includes component regulation, nanostructure design and heterostructure construction, aiming at regulating the physicochemical properties or modifying the morphology of catalysts.^{140,141} Investigations of the structure-performance relationship reveal that a structure with reasonable design is beneficial for improving the catalytic properties (Figure 13). An improved comprehension of these factors lays the groundwork for the rational design of enhanced alloy electrocatalysts in electrochemical energy conversion technologies.

4.1 | Component regulation

The intrinsic catalytic properties of electrocatalysts are heavily reliant on their elemental composition.^{62,63} Consequently, there has been extensive exploration into the modification of catalyst composition, particularly concerning transition metals, within the realm of plastic electro-reforming. Co and Ni, known for their excellent conductivity and

TABLE 2 Representative electrocatalysts for electrooxidation of plastic waste.

Electrocatalyst	Synthesis method	Morphology	Key design strategy	Ref.
CuCo ₂ O ₄ /NF	Hydrothermal and annealing	Nanowire arrays	Nanostructure control component regulation	61
Ni ₃ S ₂ (B,Co-NiS)	Hydrothermal and spontaneous reduction reaction	Defective hierarchical structure	Nanostructure control	101
CuO nanowires	In-situ self-growth method and hydrothermal reaction	Nanowires	Nanostructure control	91
Pd-NiTe/NF	Hydrothermal and wet chemical reduction	Nanoarrays	Heterostructure construction	102
0.1-CoSe ₂ /NF	Hydrothermal and annealing	Nanosheets	Nanostructure control	113
NiN ₃ -W ₅ N ₄	Hydrothermal reaction, ions exchange and nitridation	Hierarchical structure	Heterostructure construction	104
OMS-Ni ₁ -CoP	Heterogeneous nucleation, oxidation and phosphorization	Porous superstructure	Nanostructure control	105
Ni-Co ₃ -N/CC	Hydrothermal and annealing	Nanosheets	Heterostructure construction	90
CoNi _{0.2} P-uNS/NF	Hydrothermal and annealing	Ultrathin nanosheets	Nanostructure control component regulation	106
CoNi _{0.25} P/NF	Electrodeposition and annealing	Nanoparticles	Component regulation	102
MnNiCoO	Electrospinning and calcination	Porous nanofibers	Nanostructure control	108
Co-Ni ₂ P/NF	Hydrothermal and annealing	Nanosheets	Heterostructure construction	110
Pt/ γ -NiOOH/NF	Corrosion engineering	Hierarchical structure	Heterostructure construction	93
Au/Ni(OH) ₂ /NF	Electrodeposition	Hierarchical structure	Heterostructure construction	68
Pd/Ni(OH) ₂ /NF	Oxidation-reduction	Hierarchical structure	Heterostructure construction	53
Pd ₁ Ag ₁ NPs	Oxidation-reduction	Nanoparticle	Heterostructure construction	138
Ni(OH) ₂ /NF	Acid etching	Nano-layers	Nanostructure control	103
Activated nickel foam	Electro-corrosion	Nanosheets	Nanostructure control	96
Pd NTs/NF	Oxidation-reduction	Nanothorns	Nanostructure control	122
Ru-CoOOH/NF	In situ reconstruction	Nanosheets	Heterostructure construction	69
NiCo ₂ O ₄ /CFP	Hydrothermal and annealing	Nanowires	Nanostructure control	55
NiCo ₂ O ₄ /NF	Annealing	Nanosheets	Nanostructure control	98
Ni ₃ S ₂ @Fe ₂ O ₃	Hydrothermal reaction	Hierarchical structure	Heterostructure construction	97
CuCoO@rGO	NaBH ₄ reduction reaction	Hierarchical structure	Nanostructure control	127

Abbreviations: CC, carbon cloth; CFP, carbon fiber paper; NF, Ni foam; OMS, organized macroporous superstructure; uNS, ultra-thin nanosheets.

stability, have exhibited superior catalytic activity. In the pursuit of generating more active sites, catalysts based on Co, Ni, or a combination of both have been thoroughly investigated. This exploration involves introducing transition metals (e.g., Cu, Mn, Fe) or doping anion atoms (e.g., P, O, N, Se, B).

It has been demonstrated that the catalytic capability varies with the type of doped transition metals, underscoring the critical role of suitable element dopants in achieving high catalytic activity for transition metal-based electrocatalysts. For instance, different Co-based oxides (MCo₂O₄, M=Co, Ni, Fe, Cu, Zn, and Mn) were synthesized for the electrochemical conversion of PET hydrolyzates.⁹⁸ Scanning

electron microscopy (SEM) images of these Co-based oxides revealed diverse nanostructures, indicating a significant influence of the element type on the catalyst structure (Figure 14A). Notably, NiCo₂O₄ exhibited a hollow and porous structure, as evidenced by the opening area at the top, as shown in Figure 14B. This nanostructure endowed NiCo₂O₄ with the maximum electrochemically active surface area (ECSA) (Figure 14C), suggesting an abundance of active sites on its surface. Electrochemical impedance spectroscopy measurements demonstrated the lowest transfer resistance for NiCo₂O₄ (Figure 14D), indicating superior electron transfer rates during the reaction. This enhanced electron transfer can be

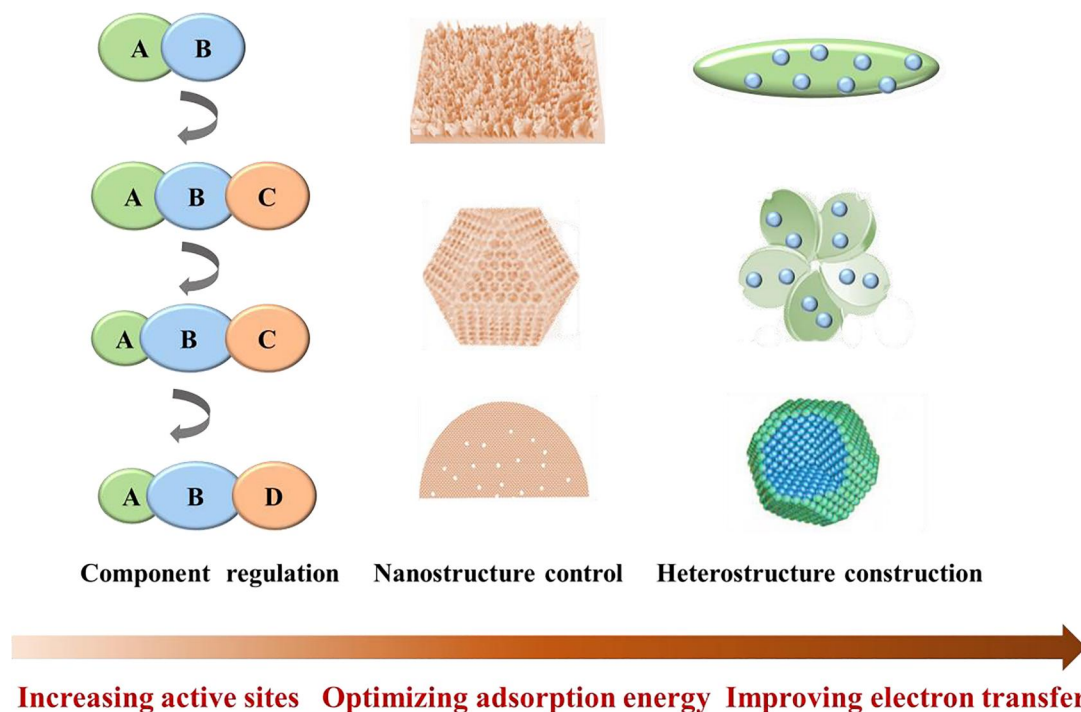


FIGURE 13 Schematic illustration of various catalyst design strategies and possible catalytic effects. The circles labeled A, B, C, and D represent different atoms, with the size of each circle corresponding to the ratio of that atom in the compound.

attributed to the multiple oxidation states of Ni. Capitalizing on the rich catalytic sites and rapid electron transport efficiency, the catalytic activity of the NiCo_2O_4 electrode surpassed that of other catalysts in the EG oxidation test. It exhibited the lowest onset potential and Tafel slope, underscoring its efficiency in promoting the electrochemical conversion of EG.

When exploring the incorporation of multiple elements into catalyst design, the species of elements also should be considered. Liu et al.⁶¹ reported the selective upcycling of plastics using Co and Cu co-doped spinel oxide supported on Ni Foam ($\text{CuCo}_2\text{O}_4/\text{NF}$), along with Co or Cu single-doped oxides (CuO and Co_3O_4). $\text{CuCo}_2\text{O}_4/\text{NF}$ exhibited the maximum ECSA and the smallest charge transfer resistance, indicative of outstanding intrinsic activity. Additionally, DFT calculations provided further perspectives into the influence of catalyst structure on the electrochemical oxidation performance of EG. Computation of the density of state and d band center of three catalysts suggested that CuCo_2O_4 exhibited a less negative d band center relative to the Fermi level than Co_3O_4 and CuO , favorable to the adsorption and activation of reactive species by inducing more empty antibonding states (Figure 14E (a)). DFT calculated binding energy of EG and OH showed that CuCo_2O_4 displayed a much smaller binding energy difference between EG^* and OH^*

(-0.4 eV) compared with Co_3O_4 and CuO (Figure 14E (b–d)), ascribed to the dual adsorption sites of EG^* on Cu and OH^* on Co. Thus, the co-doping of Co and Cu was deduced to balance the binding energy of EG^* and OH^* on the catalyst surface, promoting the simultaneous downstream reaction of EG^* and OH^* . This intricate exploration of multiple elements showcases the significance of their combination in catalyst design for optimized catalytic performance.

In the domain of crafting electrocatalysts with multiple atom modifications, the investigation of atom ratios emerges as a pivotal factor, particularly in the preparation of cobalt and nickel phosphides.^{49–51} The atom ratio plays a pivotal role in shaping the nanostructure of catalysts, thereby exerting a crucial influence on their physicochemical properties. For example, Li et al.¹¹³ prepared the cobaltous selenide (X-CoSe_2 , X represents different amounts of Se powders) by a simple hydrothermal process followed by a selenization treatment. The nanostructure of CoSe_2 altered from nanosheet to nanoparticle with the increase of Se amount from 0.1 to 0.5 g due to extra Se causing atom aggregation. Additionally, a lower Se loading of 0.02 g could not achieve the complete conversion of the catalyst precursor of $\text{Co}(\text{OH})_2$. An optimal Se amount of 0.1 g endowed the CoSe_2 with an ultrathin nanosheet of 3.5 nm, of which a monolayer with a thickness of 6–7 Å was composed of a sandwiched layer (Se–Co–Se). Consequently,

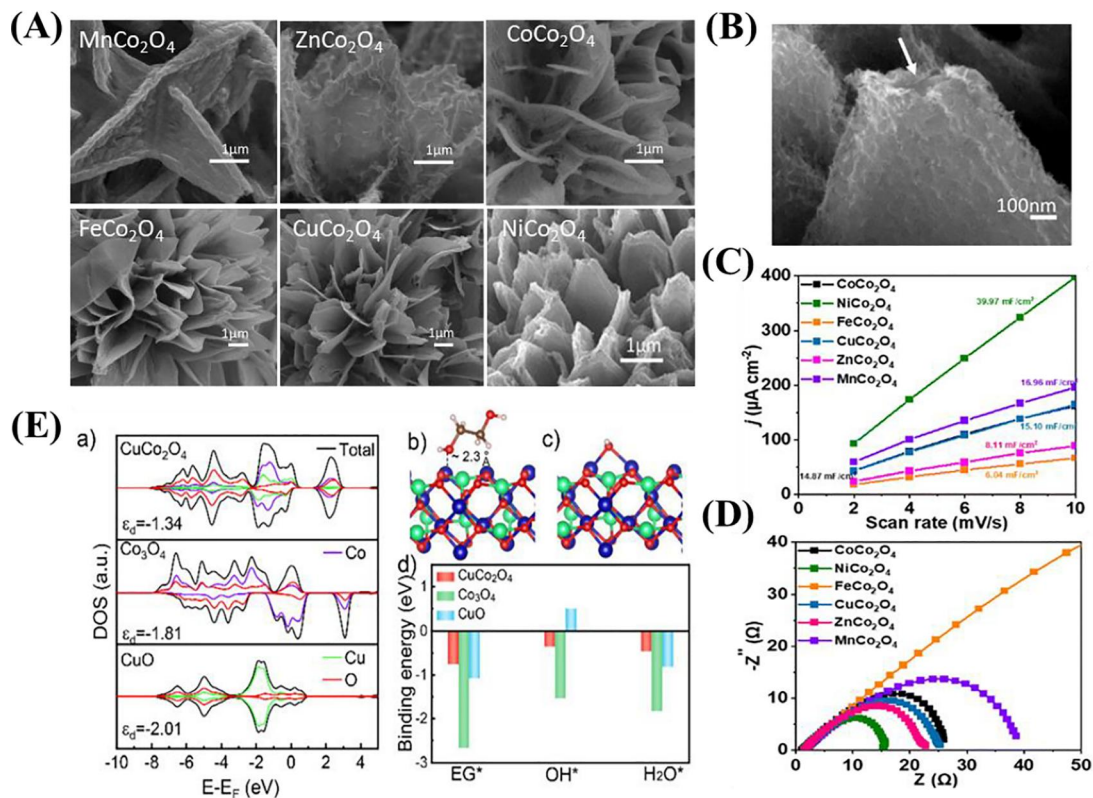


FIGURE 14 Characterizations and catalytic mechanisms of representative catalysts are designed by component regulation strategy. (A) Low-magnification SEM images of $M\text{Co}_2\text{O}_4$ ($M=\text{Co}$, Ni , Fe , Cu , Zn , and Mn). (B) High-magnification SEM image of NiCo_2O_4 . (C) Capacitive currents for different electrodes in 1 M KOH solution with 0.1 M PEF hydrolyzate. (D) Nyquist plots at the potential of 1.35 V with the $M\text{Co}_2\text{O}_4$ electrodes for the EGOR in 1 M KOH solution with 0.1 M PEF hydrolyzate. Reproduced with permission.⁹⁸ Copyright 2023, The Royal Society of Chemistry. (E) (a) Calculated DOS of CuCo_2O_4 , Co_3O_4 , and CuO . (b, c) Optimized configurations of EG^* and OH^* on the surface of CuCo_2O_4 . Blue, green, red, brown, and pink balls depict Co , Cu , O , C , and H atoms, respectively. (d) Calculated binding energies of EG , OH , and H_2O on the surfaces of CuCo_2O_4 , Co_3O_4 , and CuO . Reproduced with permission.⁶¹ Copyright 2022, The Royal Society of Chemistry. DOS, density of state; EGOR, ethylene glycol oxidation reaction; PEF, polyethylene furanoate; SEM, scanning electron microscope.

0.1- CoSe_2 nanosheets featured abundant unsaturated selenium coordination at their edges, potentially contributing to superior catalytic performance in electrocatalytic reactions.

Significantly, the precise atom ratio can give rise to unique nanostructures, such as heterostructure, and may even prompt structural reconfiguration during the catalytic process. Zhou et al.⁵⁴ engineered CoNi_xP ($x = 0, 0.1, 0.25, 0.5$, representing different feed atomic ratios of Ni/Co) and delved into the influence of atom ratios on the electrocatalyst's structure and performance. Experimental findings highlighted the superior catalytic performance of $\text{CoNi}_{0.25}\text{P}$ for HER and EGOR. This enhancement was attributed to the formation of a $\text{CoP-Ni}_2\text{P}$ hetero-junction nanostructure at the atom ratio of Ni/Co of 0.25 (Figure 15A). During the reaction process, catalyst surface reconstruction was noticed. Specifically, after the HER reaction, the transmission electron microscope (TEM) image of $\text{CoNi}_{0.25}\text{P}$ exhibited excellent preservation of both its crystalline

structure and composition (Figure 15B). Additionally, the Raman spectrum of the spent $\text{CoNi}_{0.25}\text{P}$ catalyst revealed three peaks corresponding to CoP , $\text{CoO}_x(\text{OH})_y$, and PO_x (Figure 15D), indicative of the generation of an amorphous metal oxy(hydroxide) shell structure over $\text{CoNi}_{0.25}\text{P}$. X-ray absorption near edge spectroscopy (XANES) spectra further disclosed the moderate oxidation of Co and Ni (Figure 15E), while extended X-ray absorption fine structure (EXAFS) spectra confirmed that the $\text{CoNi}_{0.25}\text{P}$ catalyst retained its primary structure during HER (Figure 15F,G). In contrast, after the EG oxidation reaction, the $\text{CoNi}_{0.25}\text{P}$ catalyst underwent a thorough reconstruction process (Figure 15C). Raman spectra of the spent $\text{CoNi}_{0.25}\text{P}$ displayed only a peak of $\text{CoO}_x(\text{OH})_y$, and the XANES spectra resembled the spectrum of the $\text{CoNi}_{0.25}\text{OOH}$ reference, as verified by the EXAFS spectra. Based on this comprehensive analysis, a proposed catalytic mechanism involved the in situ evolution of the nanostructure (Figure 15H). In detail, the bifunctional

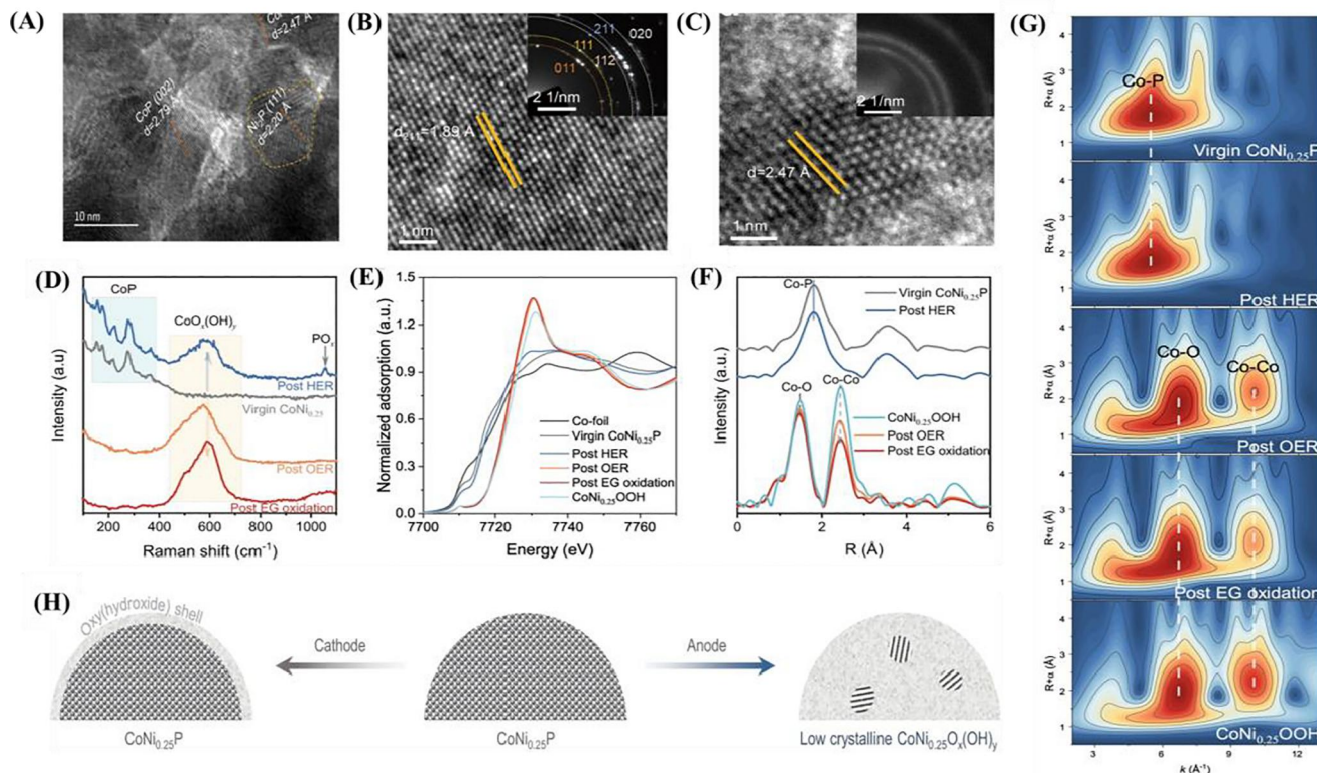


FIGURE 15 The characterizations and catalytic mechanisms of representative catalysts are designed by component regulation strategy. (A) HRTEM images of $\text{CoNi}_{0.25}\text{P}$ nanosheet. TEM images and corresponding SAED patterns of $\text{CoNi}_{0.25}\text{P}$ after HER (B) and EG oxidation (C) reaction for 1 h. (D) Raman spectra, (E) Co K-edge XANES profiles, (F) Co K-edge EXAFS spectra, and (G) wavelet transforms for Co K-edge EXAFS spectra for virgin and spent $\text{CoNi}_{0.25}\text{P}$. (H) Schematic illustration of the structural evolution of $\text{CoNi}_{0.25}\text{P}$ catalyst under reaction conditions. Reproduced with permission.⁵⁴ Copyright 2021, Spring Nature. EG, ethylene glycol; EXAFS, extended X-ray absorption fine structure; HER, hydrogen evolution reaction; HRTEM, high-resolution transmission electron microscope; OER, oxygen evolution reaction; SAED, selected area electron diffraction; TEM, transmission electron microscope; XANES, X-ray absorption near edge spectroscopy.

$\text{CoNi}_{0.25}\text{P}$ material transformed into a $\text{CoNi}_{0.25}\text{P}/\text{CoNi}_{0.25}\text{O}_x(\text{OH})_y$ core-shell structure at the cathode, while it underwent drastic oxidation and reconstruction into a low-crystalline $\text{CoNi}_{0.25}\text{O}_x(\text{OH})_y$ at the anode. This dynamic evolution provides a nuanced understanding of the catalytic mechanism of these catalysts, underscoring the importance of atom ratios in tailoring their performance.

4.2 | Nanostructure control

The morphology of electrocatalysts plays a crucial role in most electrocatalytic reactions. Novel nanostructures with special morphology could endow the catalysts with enhanced catalytic activity.¹⁴² For example, the nanostructures with high-curvature tips could promote the local electric field, thus facilitating the mass transfer during the electrocatalytic processes, which is called tip effect (TF).¹⁴³ In light of this, Ren et al.¹²² fabricated Pt nanothorns grown on the Ni foam (Pd NTs/NF), which presented the

structure of high-curvature tips on the NF surface depicted in the SEM and TEM images (Figure 16A). In contrast, Pt nanoparticles supported on the NF (Pd NPs/NF) were also obtained to explore the positive influence of TF on the catalytic efficiency of catalysts. LSV curves demonstrated that both Pd NPs/NF and Pd NTs/NF successfully facilitated the oxidation of EG to formate, whereas the conversion of EG to GA was exclusively observed in the case of Pd NTs/NF, suggesting that TF of nanostructure was critical to the preferential oxidation of EG into GA. This was attributed to the enrichment of OH^- on the tip surface of nanothorns, further accelerating the hydrogen elimination step of EG and the transformation of intermediates into GA.

Catalysts with hierarchical porous structures covering systematically arranged macropores, mesopores and micropores have shown the obvious advantages of increased active sites and boosted mass transfer.^{144,145} Wang et al.¹⁰⁵ introduced organized macroporous superstructure in the atomic Ni-anchored CoP electrocatalyst (OMS- $\text{Ni}_1\text{-CoP}$) for the

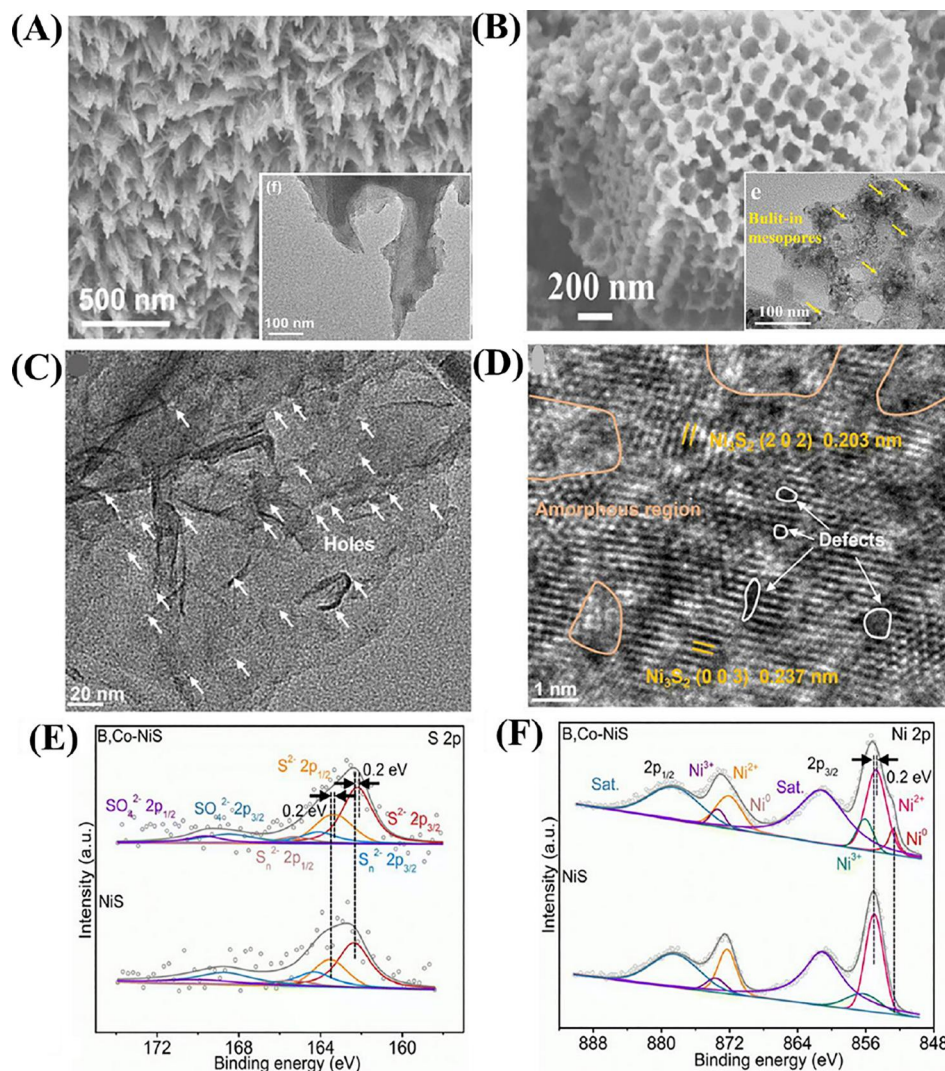


FIGURE 16 The characterizations of representative catalysts designed by nanostructure control strategy. (A) SEM image of Pd NTs/N, with the insert of TEM image. Reproduced with permission.¹²² Copyright 2023, American Chemical Society. (B) SEM image of OMS-Ni₁-CoP, with the insert of TEM image. Reproduced with permission.¹⁰⁵ Copyright 2023, Elsevier. (C) TEM image of B,Co-NiS. (D) High-resolution TEM image of B,Co-NiS. XPS spectra for (E) S 2p and (F) Ni 2p of B,Co-NiS and NiS. Reproduced with permission.¹⁰¹ Copyright 2023, The Royal Society of Chemistry. SEM, scanning electron microscope; TEM, transmission electron microscope; XPS, X-ray photoelectron spectroscopy.

electrocatalytic oxidation of PET plastic. As shown in the SEM image (Figure 16B), OMS-Ni₁-CoP presented a skeleton structure consisting of disciplined macropores and interwoven barriers, which contained a large number of built-in mesopores and perceptible Ni₁-CoP nanoparticles with a mean diameter of around 6 nm. OMS-Ni₁-CoP exhibited better catalytic activity for EGOR with a lower Tafel slope than Ni₁-CoP, indicating the critical role of OMS in the interior activity of catalyst and electron transfer in the EG oxidation process. Furthermore, it was proved that OMS also exerted a positive influence on the electrochemical reconstruction of the catalyst, thus leading to the superior performance of EGOR.

Defect engineering, which entails deliberately introducing vacancies, interstitials, dislocations, and

other imperfections onto the surface of a catalyst, has emerged as a highly effective strategy for enhancing its electrocatalytic properties.^{146–148} These intentionally engineered defects play a pivotal role in shaping the electronic structure and charge transport properties of electrocatalysts, thereby exerting significant influence on their catalytic activity, selectivity, and stability.^{149–151} For instance, Chen et al.¹⁰¹ implemented an anion–cation co-doping strategy to synthesize boron and cobalt co-doped nickel sulfide (B, Co-NiS). Throughout the NaBH₄ reduction process, Figure 16C illustrates the formation of a substantial number of voids, or “holes” in the B,Co-NiS material, while Figure 16D exposes the presence of abundant defects within the material. An EPR spectra analysis unveiled a noteworthy abundance of sulfur vacancies

in B,Co-NiS, as evidenced by the robust signal from unpaired metal-S electrons. Furthermore, XPS spectra indicated an increase in electron density around the sulfur and nickel atoms, signifying electron transfer due to the doping of boron and cobalt (Figure 16E,F). Notably, B,Co-NiS demonstrated the maximum ECSA value and the smallest charge transfer resistance value, suggesting an abundance of electroactive sites and expedited electron transfer. This comprehensive defect engineering approach not only showcases the impact on the material's structure but also highlights the resulting improvements in its electrocatalytic performance, positioning it as a promising avenue for advancements in electrochemical energy conversion technologies.

4.3 | Heterostructure construction

The concept of a heterostructure, originating from semiconductor physics, is generalized to describe a structure composed of hetero or multi-components with an active heterointerface.¹⁵² Unlike common composites, the focus of heterostructure is on the interface between multiple components rather than the components themselves. The heterointerface is classified into three types: planar interface, lateral interface and hierarchical interface.¹⁵³ While electron transmit or surface impedance may vary based on interfaces with diverse atomic arrangements, they induced analogous interface effects, primarily encompassing the electron effect and ensemble effect. The ensemble effect involves multi active sites for the adsorption and catalysis of reactants and intermediates, signifying the synergistic completion of the reaction pathway by multiple components.^{153,154} Electron effect involves the electron interaction at the interface of multi-components due to the difference in their energy band, leading to the electron redistribution of multi-components.¹⁵⁵ Electron rearrangement further alters the adsorption energy of reactants and intermediates, rendering the reaction to proceed more easily.

Planar and hierarchical interfaces, characterized by their relatively limited interfacial area, are frequently encountered in electrochemical catalysts in the field of electro-reforming of plastic waste.^{68,90,102,104} For instance, Ma et al.¹⁰⁴ synthesized the Ni₃N/W₅N₄ electrocatalyst with a unique Janus heterostructure consisting of W₅N₄ ultra-thin nanosheets and Ni₃N nanoparticles with an average of ~50 nm as shown in Figure 17A.¹⁰⁴ XPS spectra revealed that no distinct difference was observed between sole Ni₃N and W₅N₄ and Ni₃N/W₅N₄ hybrid, indicating that negligible electron transfer occurred in the heterointerface of Ni₃N and W₅N₄. It was

further proved by the ultraviolet photoelectron spectroscopy analysis that no electro was accumulated or depleted at the interface of Ni₃N and W₅N₄ due to the similar work function of ~4.79 eV (Figure 17B). As a bifunctional catalyst for HER and EGOR, the ensemble effect of Ni₃N/W₅N₄ was identified by the investigation of the hydrogen evolution pathway, which includes steps of water adsorption, water dissociation into *H, *H adsorption, and H₂ evolution (Figure 17C–E). It was demonstrated that W₅N₄ acted as water adsorption and dissociation sites while Ni₃N served as *H adsorption and H₂ evolution sites, thus the cooperation of W₅N₄ and Ni₃N boosted the reaction kinetics.

Furthermore, the electronic effect was also showcased in hierarchical Pd-NiTe/NF, characterized by its distinctive heterointerface structure between Pd nanoparticles and NiTe nanorods (Figure 17F).¹⁰² XPS analysis showed that the Ni 2p spectra and Te 3d spectra of Pd-NiTe/NF both positively shifted toward higher binding energy relative to that of the pure NiTe while the Pd 3d spectra of Pd-NiTe/NF possessed a negative deviation compared with that of the pure Pd/C (Figure 17G–I), indicating that the partial electrons were transferred from NiTe to Pd through the heterointerface. Catalytic experiments for EGOR demonstrated that the Pd-NiTe/NF exhibited superior catalytic activity than the NiTe/NF, suggesting the critical role of the heterointerface of Pd-NiTe/NF in promoting the reaction process.

Notably, both the ensemble effect and the electronic effect could occur at a heterointerface simultaneously so that the reaction kinetics and adsorption energy of intermediates could be modified to enhance the reaction efficiency. Yan et al.⁶⁸ explored the boosted capability of Au/Ni(OH)₂ with a heterointerface in comparison with pure Au and Ni(OH)₂ (Figure 17J). The adsorption energy (E_{ads}) of glycerol (similar structure with EG) on Au/Ni(OH)₂ was lower than that on pure Au and Ni(OH)₂ (Figure 17K), indicating the electron effect caused by the heterointerface. Afterward, it was proved that the adjacent OH group of glycerol interacted with the OH group of Ni(OH)₂ and Au, respectively, achieving the synergistic involvement of Au and Ni(OH)₂ through the reaction process via the ensemble effect from the interface of Au/Ni(OH)₂. Hence, the promoted activity of Au/Ni(OH)₂ was assigned to the synergistic effect of the σ bond between Au and the substrate and the hydrogen bond between Ni(OH)₂ and the substrate (Figure 17L).

In comparison to planar and hierarchical interfaces, the lateral interface exhibits a significantly increased contact area, implying a more robust interaction of electron and energy band structures between two components. Recently, Xiao et al.⁹⁷

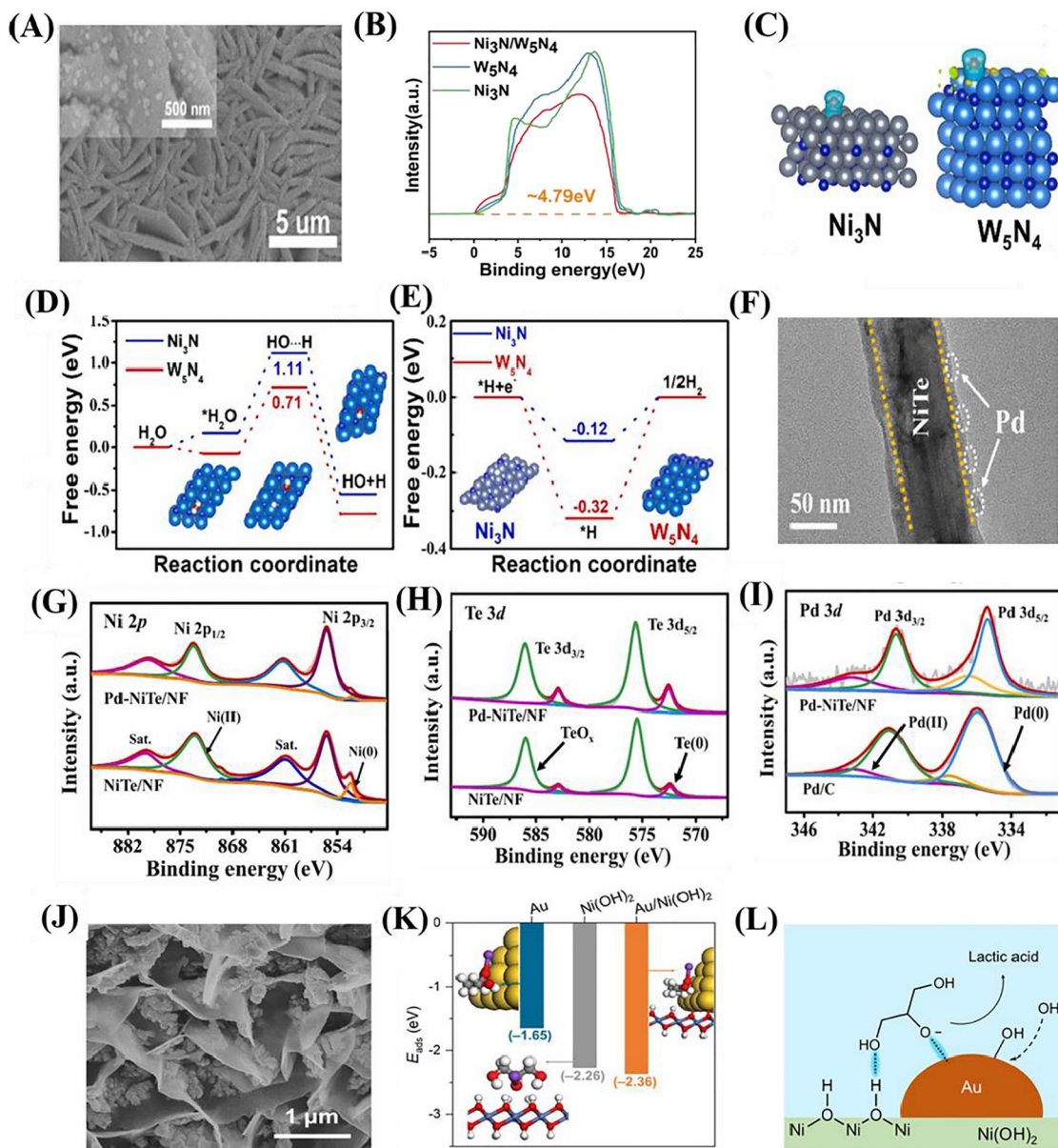


FIGURE 17 The characterizations and catalytic mechanisms of representative catalysts designed by heterostructure construction strategy. (A) SEM images of $\text{Ni}_3\text{N}/\text{W}_5\text{N}_4$. (B) UPS spectra of Ni_3N , W_5N_4 , and $\text{Ni}_3\text{N}/\text{W}_5\text{N}_4$. (C) The difference charge density of Ni_3N and W_5N_4 with adsorbed water molecules. (D) The calculated relative energy diagrams for H_2O dissociation and (E) H adsorption on Ni_3N and W_5N_4 . Reproduced with permission.¹⁰⁴ Copyright 2022, Elsevier. (F) TEM image of Pd-NiTe/NF. The high-resolution XPS spectra of (G) Ni 2p, (H) Te 3d, and (I) Pd 3d for samples. Reproduced with permission.¹⁰² Copyright 2023, Elsevier. (J) SEM image of the Au/Ni(OH)₂ catalyst. (K) Adsorption energies of glycerol in the alkoxide form on gold, nickel hydroxide, and composite Au/Ni(OH)₂, respectively. The optimized geometries of $(\text{HOCH}_2)_2\text{CH}_2\text{O}^-$ for Au, Ni(OH)₂, and Au/Ni(OH)₂ are also displayed. The color of each element is yellow for Au, blue for Ni, red for O, white for H, gray for C, and purple composite for K. (L) Graphical depiction of the adsorption conformation of glycerol alkoxide at the Au/Ni(OH)₂ junction. Reproduced with permission.⁶⁸ Copyright 2023, American Chemical Society. NF, Ni foam; SEM, scanning electron microscope; TEM, transmission electron microscope; UPS, ultraviolet photoelectron spectroscopy; XPS, X-ray photoelectron spectroscopy.

investigated the feasibility of implementing a lateral interface in the electrocatalyst designed for the oxidation of plastic. The catalyst of $\text{Ni}_3\text{S}_2@\text{Fe}_2\text{O}_3$ with core-shell heterostructure was synthesized, presenting the blossom-shaped configuration with crowdily interwoven nanosheets (Figure 18A). TEM images reveal that the Ni_3S_2 nanowalls were

enveloped by Fe_2O_3 nanoscale flakings, creating a distinctive core-shell architecture featuring a significant heterointerface contact area (Figure 18B). The core-shell architecture of $\text{Ni}_3\text{S}_2@\text{Fe}_2\text{O}_3$ was further supported by scanning transmission electron microscopy high-angle annular dark field imaging, line-scanning energy dispersive X-ray spectroscopy

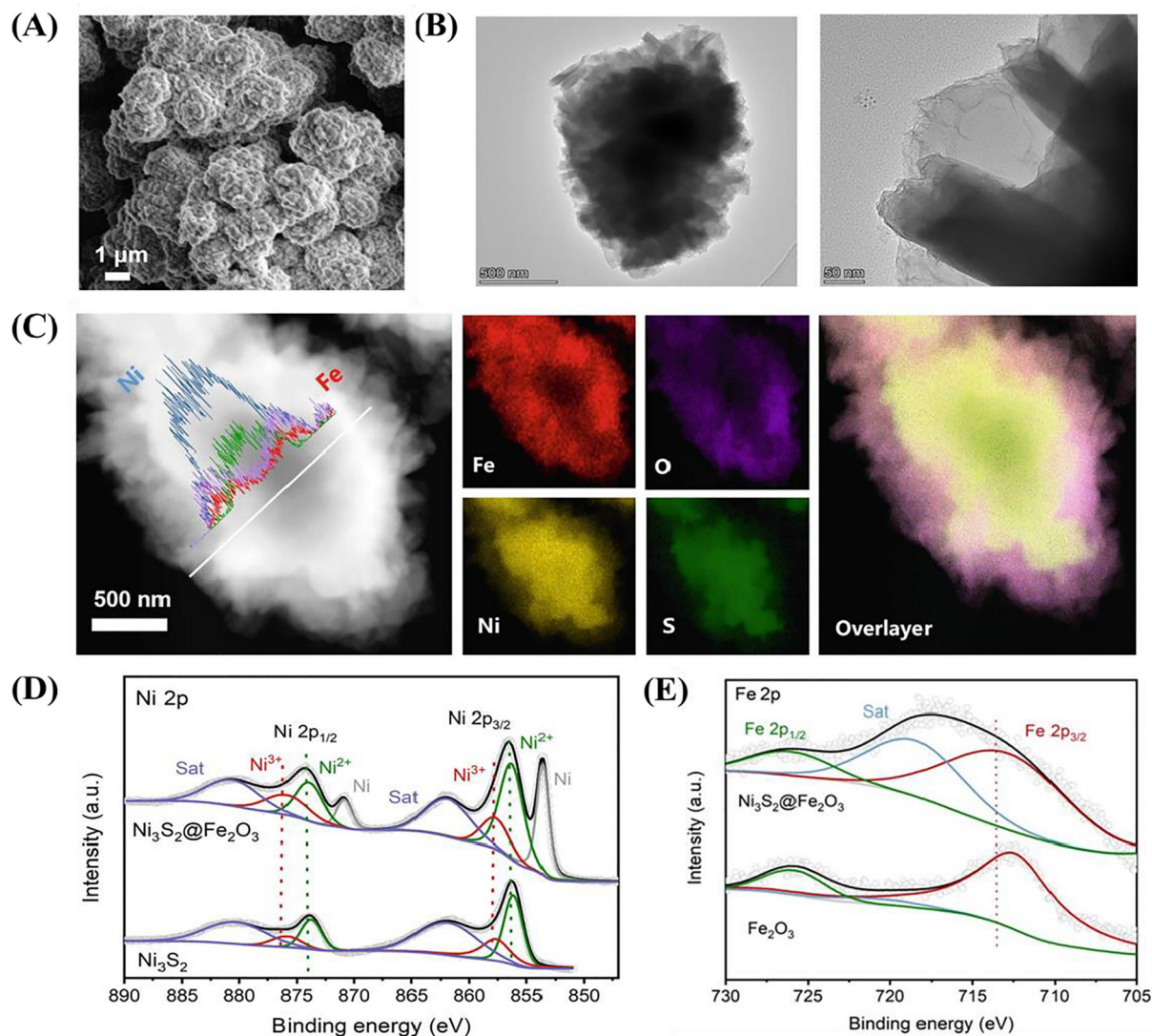


FIGURE 18 The characterizations of representative catalysts designed by heterostructure construction strategy. (A) SEM image and (B) TEM image of $\text{Ni}_3\text{S}_2@\text{Fe}_2\text{O}_3$. (C) Scanning transmission electron microscopy high-angle annular dark field image and line scanning spectra and elemental mapping images of $\text{Ni}_3\text{S}_2@\text{Fe}_2\text{O}_3$. (D) Ni 2p XPS spectra and (E) Fe 2p XPS spectra of $\text{Ni}_3\text{S}_2@\text{Fe}_2\text{O}_3$, Ni_3S_2 , and Fe_2O_3 . Reproduced with permission.⁹⁷ Copyright 2023, Wiley. SEM, scanning electron microscope; TEM, transmission electron microscope; XPS, X-ray photoelectron spectroscopy.

(EDX) spectra, and elemental mapping (Ni, Fe, O, and S) (Figure 18C). The central domain of the nanowalls exhibited the highest Ni density, gradually decreasing toward the edges, with minimal Ni detected in the nanoflake shell. Oppositely, Fe demonstrated a lower density at the center compared to the nanowall edge. The dispersion pattern of O closely mirrored that of Fe, whereas the trends for S and Ni elements were reversed. The EDX line scans images directly aligned with the elemental mapping images, providing clear confirmation that the nanoclusters consist of a Ni_3S_2 nanowall core and Fe_2O_3 nanoflakes. XPS was utilized to analyze the chemical configuration and structural alterations of $\text{Ni}_3\text{S}_2@\text{Fe}_2\text{O}_3$, Ni_3S_2 , and Fe_2O_3 . Compared with Ni_3S_2 and Fe_2O_3 , the Ni 2p and Fe 2p

peaks of $\text{Ni}_3\text{S}_2@\text{Fe}_2\text{O}_3$ both exhibited a higher energy shift, providing conclusive evidence of electron transmission between the inner Ni_3S_2 and the outer Fe_2O_3 (Figure 18D,E).

5 | CONCLUSIONS AND PERSPECTIVES

Plastic waste poses a significant environmental threat due to its extended degradation time and adverse ecological impacts. Recognizing the potential of plastic waste as a resource for valuable products is crucial. Electrocatalysis technology emerges as a promising strategy to convert plastic waste into diverse and valuable materials. However, the

exploration of this technology is still in its infancy, lacking a systematic and comprehensive understanding. To bridge this knowledge gap, this review aims to provide a thorough overview of recent advancements in electro-upgrading plastic wastes, with a specific focus on producing chemicals like FA and GA. Our exploration delves into the latest developments in diverse integration systems, emphasizing the simultaneous generation of high-value products, including but not limited to high-valued H_2 , NH_3 , hydrocarbons, and valuable anodic products. Additionally, we feature noteworthy progress in the realm of photo-electric co-electrolysis systems designed for upgrading plastic waste. These systems present a remarkable example of harnessing green energy as a sustainable alternative to conventional direct electricity inputs. The catalytic performances of electrocatalysts have attained substantial enhancements, attributed to modification engineering approaches focused on refining the structure, composition, and surface properties of catalysts. This advancement is pivotal in optimizing catalytic efficiency and enhancing the overall electro-upgrading process. From an economic standpoint, this promising field of electro-reforming for upgrading plastic waste toward esteemed commodities deserves wider exploration.

5.1 | Scaling PET electrolysis systems for industrial application

Advancements in the electrochemical upgrading of plastic waste, particularly PET, have demonstrated promising results at the laboratory scale. The shift toward large-scale industrial processes is imperative for the practical implementation of plastic waste electrolysis. It is essential to address challenges associated with ensuring the stability of catalysts and seamless system integration. Overcoming these hurdles is paramount to realizing the practical viability of electrolysis on an industrial scale for effective plastic waste management. A collaborative effort in this direction could significantly contribute to the industrial adoption of electrolysis for plastic waste treatment. Additionally, exploring the potential of other plastic types for industrial applications should be considered, expanding the scope of sustainable waste management solutions.

5.2 | Innovative electrocatalysts for enhanced formic acid formation

Transitional metals like Co and Ni are pivotal in designing electrocatalysts for FA. Despite enhanced performance in electrochemical conversion, the

operating potential remains high. To tackle this issue, a strategic approach involves refining catalysts through modification engineering techniques like nanocomposites and introducing other transitional metals. Emphasizing catalyst regulation to mitigate the OER process under high potential is pivotal for boosting overall reaction efficiency. This research trajectory holds significant promise in enhancing the effectiveness of electrocatalysts, thereby contributing to the development of more sustainable and economically viable electrochemical processes for FA production.

5.3 | Inventive integration systems for diverse cathodic reactions

The prevailing research on integration systems has predominantly centered on the coupling of plastic oxidation with hydrogen production. However, delving into innovative cathodic reactions such as CO_2 reduction, NO_3^- reduction, N_2 reduction, and HMF reduction represents an underexplored frontier. These alternative reactions not only contribute to the disposal of environmental pollutants but also offer the potential to generate value-added chemicals and energy sources. A more in-depth exploration of these alternative reactions holds the promise of uncovering novel pathways for converting plastic waste into valuable resources, thereby expanding the horizons and possibilities in the realm of waste management.

5.4 | Heightened focus on high-valued glycolic acid production

The electrochemical synthesis of GA encounters obstacles related to the scarcity of noble metal catalysts and elevated overpotential. Despite these challenges, the market value of GA remains substantial. Future research endeavors should prioritize the development of cost-effective electrocatalysts, with a dedicated focus on enhancing selectivity for GA. Additionally, exploring synergies by integrating GA production with other valuable chemicals is paramount. This strategic emphasis is poised to expedite progress in GA production technology, ensuring not only higher yield and purity but also promoting overall sustainability in the process.

5.5 | Renewable energy-driven electrolysis for sustainable plastic waste treatment

While electro-upgrading of plastic waste operates under mild conditions, substantial electricity

consumption remains a concern. Introducing green electricity from renewable sources such as wind, water, and solar power can enhance the environmental sustainability of the electrocatalysis system. This shift reduces reliance on conventional non-renewable electricity, aligning with broader goals of reducing carbon footprints. Incorporating green electricity into electro-upgrading processes contributes to a more eco-friendly and energy-efficient approach to managing global plastic waste.

ACKNOWLEDGMENTS

This work is supported by the Australian Research Council (ARC) Discovery Project (DP220101139).

CONFLICT OF INTEREST STATEMENT

The authors declare no conflict of interest.

ORCID

Zhijie Chen  <https://orcid.org/0000-0003-0627-0856>

REFERENCES

- Chen J, Zhang L, Wang L, Kuang M, Wang S, Yang J. Toward carbon neutrality: selective conversion of waste plastics into value-added chemicals. *Matter*. 2023;6:3322-3347. <https://doi.org/10.1016/j.matt.2023.07.025>
- Yu J, Sun L, Ma C, Qiao Y, Yao H. Thermal degradation of PVC: a review. *Waste Manag*. 2016;48:300-314. <https://doi.org/10.1016/j.wasman.2015.11.041>
- Agrawala S, Lanzi E, Dellink R. *Global Plastics Outlook: Policy Scenarios to 2060*. OECD Publishing; 2022.
- Barnes DKA, Galgani F, Thompson RC, Barlaz M. Accumulation and fragmentation of plastic debris in global environments. *Phil Trans Roy Soc B*. 2009;364(1526):1985-1998. <https://doi.org/10.1098/rstb.2008.0205>
- Law KL, Thompson RC. Microplastics in the seas. *Science*. 2014;345(6193):144-145. <https://doi.org/10.1126/science.1254065>
- Cornwall W. The plastic eaters. *Science*. 2021;373(6550):36-39. <https://doi.org/10.1126/science.373.6550.36>
- MacLeod M, Arp HPH, Tekman MB, Jahnke A. The global threat from plastic pollution. *Science*. 2021;373(6550):61-65. <https://doi.org/10.1126/science.abg5433>
- Williams J. The new plastic economy. *Ecogeneration*. 2017;58. <https://doi.org/10.3316/informit.627029506816409>
- Pivokonsky M, Cermakova L, Novotna K, Peer P, Cajthaml T, Janda V. Occurrence of microplastics in raw and treated drinking water. *Sci Total Environ*. 2018;643:1644-1651. <https://doi.org/10.1016/j.scitotenv.2018.08.102>
- Ivleva NP, Wiesheu AC, Niessner R. Microplastic in aquatic ecosystems. *Angew Chem Int Ed*. 2017;56(7):1720-1739. <https://doi.org/10.1002/anie.201606957>
- Chen Z, Liu X, Wei W, Chen H, Ni B-J. Removal of microplastics and nanoplastics from urban waters: separation and degradation. *Water Res*. 2022;221:118820. <https://doi.org/10.1016/j.watres.2022.118820>
- Chen Z, Shi X, Zhang J, Wu L, Wei W, Ni B-J. Nanoplastics are significantly different from microplastics in urban waters. *Water Res*. 2023;19:100169. <https://doi.org/10.1016/j.wroa.2023.100169>
- Rahimi A, Garcia JM. Chemical recycling of waste plastics for new materials production. *Nat Rev Chem*. 2017;1(6):0046. <https://doi.org/10.1038/s41570-017-0046>
- Raheem AB, Noor ZZ, Hassan A, Abd Hamid MK, Samsudin SA, Sabeen AH. Current developments in chemical recycling of post-consumer polyethylene terephthalate wastes for new materials production: a review. *J Clean Prod*. 2019;225:1052-1064. <https://doi.org/10.1016/j.jclepro.2019.04.019>
- Ren W, Zhou P, Nie G, et al. Hydroxyl radical dominated elimination of plasticizers by peroxymonosulfate on metal-free boron: kinetics and mechanisms. *Water Res*. 2020;186:116361. <https://doi.org/10.1016/j.watres.2020.116361>
- Anjana K, Hinduja M, Sujitha K, Dharani G. Review on plastic wastes in marine environment – biodegradation and biotechnological solutions. *Mar Pollut Bull*. 2020;150:110733. <https://doi.org/10.1016/j.marpolbul.2019.110733>
- Chen Z, Wei W, Liu X, Ni B-J. Emerging electrochemical techniques for identifying and removing micro/nanoplastics in urban waters. *Water Res*. 2022;221:118846. <https://doi.org/10.1016/j.watres.2022.118846>
- Zhuo M, Chen Z, Liu X, Wei W, Shen Y, Ni B-J. A broad horizon for sustainable catalytic oxidation of microplastics. *Environ Pollut*. 2024;340:122835. <https://doi.org/10.1016/j.envpol.2023.122835>
- Schyns ZOG, Shaver MP. Mechanical recycling of packaging plastics: a review. *Macromol Rapid Commun*. 2021;42(3):2000415. <https://doi.org/10.1002/marc.202000415>
- Ragaert K, Delva L, Van Geem K. Mechanical and chemical recycling of solid plastic waste. *Waste Manag*. 2017;69:24-58. <https://doi.org/10.1016/j.wasman.2017.07.044>
- Sardon H, Dove AP. Plastics recycling with a difference. *Science*. 2018;360(6387):380-381. <https://doi.org/10.1126/science.aat4997>
- Liu B, Lu X, Ju Z, et al. Ultrafast homogeneous glycolysis of waste polyethylene terephthalate via a dissolution-degradation strategy. *Ind Eng Chem Res*. 2018;57(48):16239-16245. <https://doi.org/10.1021/acs.iecr.8b03854>
- Jing Y, Wang Y, Furukawa S, et al. Toward the circular economy: converting aromatic plastic waste back to arenes over a Ru/Nb₂O₅ catalyst. *Angew Chem Int Ed*. 2021;60(10):5527-5535. <https://doi.org/10.1002/anie.202011063>
- Demarteau J, O'Harra KE, Bara JE, Sardon H. Valorization of plastic wastes for the synthesis of imidazolium-based self-supported elastomeric ionenes. *ChemSusChem*. 2020;13(12):3122-3126. <https://doi.org/10.1002/cssc.202000505>
- Quaranta E, Dibenedetto A, Nocito F, Fini P. Chemical recycling of poly-(bisphenol A carbonate) by diaminolysis: a new carbon-saving synthetic entry into non-isocyanate polyureas (NIPUreas). *J Hazard Mater*. 2021;403:123957. <https://doi.org/10.1016/j.jhazmat.2020.123957>
- Kumar A, von Wolff N, Rauch M, et al. Hydrogenative depolymerization of nylons. *J Am Chem Soc*. 2020;142(33):14267-14275. <https://doi.org/10.1021/jacs.0c05675>
- Fuentes JA, Smith SM, Scharbert MT, et al. On the functional group tolerance of ester hydrogenation and polyester depolymerisation catalysed by Ruthenium complexes of tridentate aminophosphine ligands. *Chem-Eur J*. 2015;21(30):10851-10860. <https://doi.org/10.1002/chem.201500907>
- Westhues S, Idel J, Klankermayer J. Molecular catalyst systems as key enablers for tailored polyesters and polycarbonate recycling concepts. *Sci Adv*. 2018;4(8):eaat9669. <https://doi.org/10.1126/sciadv.aat9669>
- Chen G, Li X, Feng X. Upgrading organic compounds through the coupling of electrooxidation with hydrogen evolution. *Angew Chem Int Ed*. 2022;61(42):e202209014. <https://doi.org/10.1002/anie.202209014>
- Chen Z, Wei W, Song L, Ni B-J. Hybrid water electrolysis: a new sustainable avenue for energy-saving hydrogen production. *Sustain Horiz*. 2022;1:100002. <https://doi.org/10.1016/j.horiz.2021.100002>

31. Zhou Y, Rodríguez-López J, Moore JS. Heterogenous electromediated depolymerization of highly crystalline polyoxymethylene. *Nat Commun.* 2023;14(1):4847. <https://doi.org/10.1038/s41467-023-39362-z>
32. Tee SY, Win KY, Teo WS, et al. Recent progress in energy-driven water splitting. *Adv Sci.* 2017;4(5):1600337. <https://doi.org/10.1002/advs.201600337>
33. Wu D, Kusada K, Yoshioka S, et al. Efficient overall water splitting in acid with anisotropic metal nanosheets. *Nat Commun.* 2021;12(1):1145. <https://doi.org/10.1038/s41467-021-20956-4>
34. Zhuang Z, Wang Y, Xu C-Q, et al. Three-dimensional open nano-netcage electrocatalysts for efficient pH-universal overall water splitting. *Nat Commun.* 2019;10(1):4875. <https://doi.org/10.1038/s41467-019-12885-0>
35. Dotan H, Landman A, Sheehan SW, et al. Decoupled hydrogen and oxygen evolution by a two-step electrochemical-chemical cycle for efficient overall water splitting. *Nat Energy.* 2019;4(9):786-795. <https://doi.org/10.1038/s41560-019-0462-7>
36. Wolff CM, Frischmann PD, Schulze M, et al. All-in-one visible-light-driven water splitting by combining nanoparticulate and molecular co-catalysts on CdS nanorods. *Nat Energy.* 2018;3(10):862-869. <https://doi.org/10.1038/s41560-018-0229-6>
37. Qian Q, He X, Li Z, et al. Electrochemical biomass upgrading coupled with hydrogen production under industrial-level current density. *Adv Mater.* 2023;35(25):2300935. <https://doi.org/10.1002/adma.202300935>
38. Chen Z, Liu Y, Wei W, Ni B-J. Recent advances in electrocatalysts for halogenated organic pollutant degradation. *Environ Sci Nano.* 2019;6(8):2332-2366. <https://doi.org/10.1039/C9EN00411D>
39. Gong K, Du F, Xia Z, Durstock M, Dai L. Nitrogen-doped carbon nanotube arrays with high electrocatalytic activity for oxygen reduction. *Science.* 2009;323(5915):760-764. <https://doi.org/10.1126/science.1168049>
40. Chen Z, Han N, Zheng R, Ren Z, Wei W, Ni B. Design of earth-abundant amorphous transition metal-based catalysts for electrooxidation of small molecules: advances and perspectives. *SusMat.* 2023;3:290-319. <https://doi.org/10.1002/sus2.131>
41. Chen Z, Zheng R, Wei W, Ni B-J, Chen H. Unlocking the electrocatalytic activity of natural chalcopyrite using mechanochemistry. *J Energy Chem.* 2022;68:275-283. <https://doi.org/10.1016/j.jechem.2021.11.005>
42. Li R, Xiang K, Peng Z, Zou Y, Wang S. Recent advances on electrolysis for simultaneous generation of valuable chemicals at both anode and cathode. *Adv Energy Mater.* 2021;11(46):2102292. <https://doi.org/10.1002/aenm.202102292>
43. Wang D, Wang P, Wang S, Chen Y-H, Zhang H, Lei A. Direct electrochemical oxidation of alcohols with hydrogen evolution in continuous-flow reactor. *Nat Commun.* 2019;10(1):2796. <https://doi.org/10.1038/s41467-019-10928-0>
44. Liang Z, Jiang D, Wang X, et al. Molecular engineering to tune the ligand environment of atomically dispersed nickel for efficient alcohol electrochemical oxidation. *Adv Funct Mater.* 2021;31(51):2106349. <https://doi.org/10.1002/adfm.202106349>
45. Chen Z, Wei W, Ni B-J. Transition metal chalcogenides as emerging electrocatalysts for urea electrolysis. *Curr Opin Electrochem.* 2022;31:100888. <https://doi.org/10.1016/j.coelec.2021.100888>
46. Chen Z, Wei W, Shon HK, Ni B-J. Designing bifunctional catalysts for urea electrolysis: progress and perspectives. *Green Chem.* 2024;26:631-654. <https://doi.org/10.1039/d3gc03329e>
47. Chen Z, Zheng R, Zou H, et al. Amorphous iron-doped nickel boride with facilitated structural reconstruction and dual active sites for efficient urea electrooxidation. *Chem Eng J.* 2023;465:142684. <https://doi.org/10.1016/j.cej.2023.142684>
48. Luo H, Barrio J, Sunny N, et al. Progress and perspectives in photo- and electrochemical-oxidation of biomass for sustainable chemicals and hydrogen production. *Adv Energy Mater.* 2021;11(43):2101180. <https://doi.org/10.1002/aenm.202101180>
49. Lucas FWS, Grim RG, Tacey SA, et al. Electrochemical routes for the valorization of biomass-derived feedstocks: from chemistry to application. *ACS Energy Lett.* 2021;1205-1270. <https://doi.org/10.1021/acseenergylett.0c02692>
50. Liu W-J, Dang L, Xu Z, Yu H-Q, Jin S, Huber GW. Electrochemical oxidation of 5-hydroxymethylfurfural with NiFe layered double hydroxide (LDH) nanosheet catalysts. *ACS Catal.* 2018;8(6):5533-5541. <https://doi.org/10.1021/acscatal.8b01017>
51. Zhang N, Zou Y, Tao L, et al. Electrochemical oxidation of 5-hydroxymethylfurfural on nickel nitride/carbon nanosheets: reaction pathway determined by in situ sum frequency generation vibrational spectroscopy. *Angew Chem Int Ed.* 2019;131(44):16042-16050. <https://doi.org/10.1002/ange.201908722>
52. Chen Z, Zheng R, Bao T, et al. Dual-doped nickel sulfide for electro-upgrading polyethylene terephthalate into valuable chemicals and hydrogen fuel. *Nano-Micro Lett.* 2023;15(1):210. <https://doi.org/10.1007/s40820-023-01181-8>
53. Liu F, Gao X, Shi R, Guo Z, Tse ECM, Chen Y. Concerted and selective electrooxidation of polyethylene-terephthalate-derived alcohol to glycolic acid at an industry-level current density over a Pd-Ni(OH)₂ catalyst. *Angew Chem Int Ed.* 2023;62(11):e202300094. <https://doi.org/10.1002/anie.202300094>
54. Zhou H, Ren Y, Li Z, et al. Electrocatalytic upcycling of polyethylene terephthalate to commodity chemicals and H₂ fuel. *Nat Commun.* 2021;12(1):4679. <https://doi.org/10.1038/s41467-021-25048-x>
55. Wang J, Li X, Wang M, et al. Electrocatalytic valorization of poly(ethylene terephthalate) plastic and CO₂ for simultaneous production of formic acid. *ACS Catal.* 2022;12(11):6722-6728. <https://doi.org/10.1021/acscatal.2c01128>
56. Mishra S, Goje AS. Chemical recycling, kinetics, and thermodynamics of alkaline depolymerization of waste poly(ethylene terephthalate) (PET). *Polym React Eng.* 2003;11(4):963-987. <https://doi.org/10.1081/PRE-120026382>
57. Barredo A, Asueta A, Amundarain I, et al. Chemical recycling of monolayer PET tray waste by alkaline hydrolysis. *J Environ Chem Eng.* 2023;11(3):109823. <https://doi.org/10.1016/j.jecec.2023.109823>
58. Yue H, Zhao Y, Ma X, Gong J. Ethylene glycol: properties, synthesis, and applications. *Chem Soc Rev.* 2012;41(11):4218-4244. <https://doi.org/10.1039/C2CS15359A>
59. Zhang Z, Huber GW. Catalytic oxidation of carbohydrates into organic acids and furan chemicals. *Chem Soc Rev.* 2018;47(4):1351-1390. <https://doi.org/10.1039/c7cs00213k>
60. Xin L, Zhang Z, Qi J, Chadderdon D, Li W. Electrocatalytic oxidation of ethylene glycol (EG) on supported Pt and Au catalysts in alkaline media: reaction pathway investigation in three-electrode cell and fuel cell reactors. *Appl Catal B Environ.* 2012;125:85-94. <https://doi.org/10.1016/j.apcatb.2012.05.024>
61. Liu F, Gao X, Shi R, Tse ECM, Chen Y. A general electrochemical strategy for upcycling polyester plastics into added-value chemicals by a CuCo₂O₄ catalyst. *Green Chem.* 2022;24(17):6571-6577. <https://doi.org/10.1039/D2GC02049A>
62. Zhang AY, Sun Z, Joe Leung CC, et al. Valorisation of bakery waste for succinic acid production. *Green Chem.* 2013;15(3):690-695. <https://doi.org/10.1039/C2GC36518A>
63. Debe MK. Electrocatalyst approaches and challenges for automotive fuel cells. *Nature.* 2012;486(7401):43-51. <https://doi.org/10.1038/nature11115>

64. Lu Q, Rosen J, Zhou Y, et al. A selective and efficient electrocatalyst for carbon dioxide reduction. *Nat Commun.* 2014;5(1):3242. <https://doi.org/10.1038/ncomms4242>
65. Li L, Wang P, Shao Q, Huang X. Recent progress in advanced electrocatalyst design for acidic oxygen evolution reaction. *Adv Mater.* 2021;33(50):2004243. <https://doi.org/10.1002/adma.202004243>
66. Chen Z, Zheng R, Deng S, et al. Modular design of an efficient heterostructured FeS₂/TiO₂ oxygen evolution electrocatalyst via sulfidation of natural ilmenites. *J Mater Chem A.* 2021;9(44):25032-25041. <https://doi.org/10.1039/d1ta08168c>
67. Chen Z, Wei W, Chen H, Ni B-J. Eco-designed electrocatalysts for water splitting: a path toward carbon neutrality. *Int J Hydrogen Energy.* 2023;48(16):6288-6307. <https://doi.org/10.1016/j.ijhydene.2022.03.046>
68. Yan Y, Zhou H, Xu S-M, et al. Electrocatalytic upcycling of biomass and plastic wastes to biodegradable polymer monomers and hydrogen fuel at high current densities. *J Am Chem Soc.* 2023;145(11):6144-6155. <https://doi.org/10.1021/jacs.2c11861>
69. Ren T, Yu Z, Yu H, et al. Sustainable ammonia electrosynthesis from nitrate wastewater coupled to electrocatalytic upcycling of polyethylene terephthalate plastic waste. *ACS Nano.* 2023;17(13):12422-12432. <https://doi.org/10.1021/acsnano.3c01862>
70. Miao Y, Zhao Y, Zhang S, Shi R, Zhang T. Strain engineering: a boosting strategy for photocatalysis. *Adv Mater.* 2022;34(2022):2200868. <https://doi.org/10.1002/adma.202200868>
71. Yan Y, Wang P, Lin J, Cao J, Qi J. Modification strategies on transition metal-based electrocatalysts for efficient water splitting. *J Energy Chem.* 2021;58:446-462. <https://doi.org/10.1016/j.jechem.2020.10.010>
72. Sun J, Zhou Y, Zhao Z, Meng X, Li Z. Modification strategies to improve electrocatalytic activity in seawater splitting: a review. *J Mater Sci.* 2022;57(41):19243-19259. <https://doi.org/10.1007/s10853-022-07875-5>
73. Cheng R, Min Y, Li H, Fu C. Electronic structure regulation in the design of low-cost efficient electrocatalysts: from theory to applications. *Nano Energy.* 2023;115:108718. <https://doi.org/10.1016/j.nanoen.2023.108718>
74. Cao X, Huo J, Li L, et al. Recent advances in engineered Ru-based electrocatalysts for the hydrogen/oxygen conversion reactions. *Adv Energy Mater.* 2022;12(41):2202119. <https://doi.org/10.1002/aenm.202202119>
75. Mancini SD, Zanin M. Optimization of neutral hydrolysis reaction of post-consumer PET for chemical recycling. *Prog Rubber Plast Recycl Technol.* 2004;20(2):117-132. <https://doi.org/10.1177/147776060402000202>
76. Kawai F, Kawabata T, Oda M. Current knowledge on enzymatic PET degradation and its possible application to waste stream management and other fields. *Appl Microbiol Biotechnol.* 2019;103(11):4253-4268. <https://doi.org/10.1007/s00253-019-09717-y>
77. Yoshioka T, Sato T, Okuwaki A. Hydrolysis of waste PET by sulfuric acid at 150°C for a chemical recycling. *J Appl Polym Sci.* 1994;52(9):1353-1355. <https://doi.org/10.1002/app.1994.070520919>
78. Karayannidis GP, Chatziavgoustis AP, Achilias DS. Poly(ethylene terephthalate) recycling and recovery of pure terephthalic acid by alkaline hydrolysis. *Adv Polym Technol.* 2002;21(4):250-259. <https://doi.org/10.1002/adv.10029>
79. Barnard E, Rubio Arias JJ, Thielemans W. Chemolytic depolymerisation of PET: a review. *Green Chem.* 2021;23(11):3765-3789. <https://doi.org/10.1039/D1GC00887K>
80. Paliwal NR, Mungray AK. Ultrasound assisted alkaline hydrolysis of poly(ethylene terephthalate) in presence of phase transfer catalyst. *Polym Degrad Stabil.* 2013;98(10):2094-2101. <https://doi.org/10.1016/j.polymdegradstab.2013.06.030>
81. Yamashita M, Mukai H. Alkaline hydrolysis of polyethylene terephthalate at lower reaction temperature. *Sci Eng Rev Doshisha Univ.* 2011;52:51-56.
82. Ügdüler S, Van Geem KM, Denolf R, et al. Toward closed-loop recycling of multilayer and coloured PET plastic waste by alkaline hydrolysis. *Green Chem.* 2020;22(16):5376-5394. <https://doi.org/10.1039/D0GC00894J>
83. Aguado A, Martínez L, Becerra L, et al. Chemical depolymerisation of PET complex waste: hydrolysis vs. glycolysis. *J Mater Cycles Waste Manag.* 2014;16(2):201-210. <https://doi.org/10.1007/s10163-013-0177-y>
84. Carta D, Cao G, D'Angeli C. Chemical recycling of poly(ethylene terephthalate) (PET) by hydrolysis and glycolysis. *Environ Sci Pollut Control Ser.* 2003;10(6):390-394. <https://doi.org/10.1065/espr2001.12.104.8>
85. Bulushev DA, Ross JRH. Towards sustainable production of formic acid. *ChemSusChem.* 2018;11(5):821-836. <https://doi.org/10.1002/cssc.201702075>
86. Millet DB, Baasandorj M, Farmer DK, et al. A large and ubiquitous source of atmospheric formic acid. *Atmos Chem Phys.* 2015;15(11):6283-6304. <https://doi.org/10.5194/acp-15-6283-2015>
87. Chen X, Liu Y, Wu J. Sustainable production of formic acid from biomass and carbon dioxide. *Mol Catal.* 2020;483:110716. <https://doi.org/10.1016/j.mcat.2019.110716>
88. Rumayor M, Dominguez-Ramos A, Irabien A. Formic acid manufacture: carbon dioxide utilization alternatives. *Appl Sci.* 2018;8(6):914. <https://doi.org/10.3390/app8060914>
89. Ramulifho T, Ozoemena KI, Modibedi RM, Jafta CJ, Mathe MK. Electrocatalytic oxidation of ethylene glycol at palladium-bimetallic nanocatalysts (PdSn and PdNi) supported on sulfonate-functionalised multi-walled carbon nanotubes. *J Electroanal Chem.* 2013;692:26-30. <https://doi.org/10.1016/j.jelechem.2012.12.010>
90. Liu X, Fang Z, Xiong D, et al. Upcycling PET in parallel with energy-saving H₂ production via bifunctional nickel-cobalt nitride nanosheets. *Nano Res.* 2023;16(4):4625-4633. <https://doi.org/10.1007/s12274-022-5085-9>
91. Wang J, Li X, Zhang T, Chen Y, Wang T, Zhao Y. Electro-reforming polyethylene terephthalate plastic to co-produce valued chemicals and green hydrogen. *J Phys Chem Lett.* 2022;13(2):622-627. <https://doi.org/10.1021/acs.jpcclett.1c03658>
92. Zhao X, Boruah B, Chin KF, Đokić M, Modak JM, Soo HS. Upcycling to sustainably reuse plastics. *Adv Mater.* 2022;34(25):2100843. <https://doi.org/10.1002/adma.202100843>
93. Du M, Zhang Y, Kang S, et al. Electrochemical production of glycolate fuelled by polyethylene terephthalate plastics with improved techno-economics. *Small.* 2023;19(39):2303693. <https://doi.org/10.1002/smll.202303693>
94. Eerhart AJJE, Faaij APC, Patel MK. Replacing fossil based PET with biobased PEF; process analysis, energy and GHG balance. *Energy Environ Sci.* 2012;5(4):6407-6422. <https://doi.org/10.1039/C2EE02480B>
95. Hwang K-R, Jeon W, Lee SY, Kim M-S, Park Y-K. Sustainable bioplastics: recent progress in the production of bio-building blocks for the bio-based next-generation polymer PEF. *Chem Eng J.* 2020;390:124636. <https://doi.org/10.1016/j.cej.2020.124636>
96. Liu X, Wang J, Fang Z, et al. Ultrafast activation of Ni foam by electro-corrosion and its use for upcycling PBT plastic waste. *Appl Catal B Environ.* 2023;334:122870. <https://doi.org/10.1016/j.apcatb.2023.122870>
97. Xiao C, Leow WR, Chen L, Li Y, Li C. Electrocatalytic conversion of waste polyamide-66 hydrolysates into high-added-value adiponitrile and hydrogen fuel. *Electron.* 2023;1(2):e14. <https://doi.org/10.1002/elt2.14>
98. Ren L, Yang S, Wang J, et al. Electrocatalytic valorization of waste polyethylene furanoate (PEF) bioplastics for the

- production of formic acid and hydrogen energy. *React Chem Eng J.* 2023;8:1937-1942. <https://doi.org/10.1039/D3RE00028A>
99. de Jong E, Visser A, Dias AS, Harvey C, Gruter G-JM. The road to bring FDCA and PEF to the market. *Polymers.* 2022; 14(5):943. <https://doi.org/10.3390/polym14050943>
 100. Pichler CM, Bhattacharjee S, Rahaman M, Uekert T, Reisner E. Conversion of polyethylene waste into gaseous hydrocarbons via integrated tandem chemical-photo/electrocatalytic processes. *ACS Catal.* 2021;11(15):9159-9167. <https://doi.org/10.1021/acscatal.1c02133>
 101. Chen Z, Wei W, Shen Y, Ni B-J. Defective nickel sulfide hierarchical structures for efficient electrochemical conversion of plastic waste to value-added chemicals and hydrogen fuel. *Green Chem.* 2023;25(15):5979-5988. <https://doi.org/10.1039/D3GC01499A>
 102. Zhang H, Wang Y, Li X, et al. Electrocatalytic upcycling of polyethylene terephthalate plastic to formic acid coupled with energy-saving hydrogen production over hierarchical Pd-doped NiTe nanoarrays. *Appl Catal B Environ.* 2024;340: 123236. <https://doi.org/10.1016/j.apcatb.2023.123236>
 103. Liu K, Wang Y, Liu F, Liu C, Shi R, Chen Y. Selective electrocatalytic reforming of PET-derived ethylene glycol to formate with a Faraday efficiency of 93.2% at industrial-level current densities. *Chem Eng J.* 2023;473:145292. <https://doi.org/10.1016/j.cej.2023.145292>
 104. Ma F, Wang S, Gong X, et al. Highly efficient electrocatalytic hydrogen evolution coupled with upcycling of microplastics in seawater enabled via Ni₃N/W₅N₄ janus nanostructures. *Appl Catal B Environ.* 2022;307:121198. <https://doi.org/10.1016/j.apcatb.2022.121198>
 105. Wang N, Li X, Hu M-K, et al. Ordered macroporous superstructure of bifunctional cobalt phosphide with heteroatomic modification for paired hydrogen production and polyethylene terephthalate plastic recycling. *Appl Catal B Environ.* 2022;316:121667. <https://doi.org/10.1016/j.apcatb.2022.121667>
 106. Wang X-H, Zhang Z-N, Wang Z, et al. Ultra-thin CoNi_{0.2}P nanosheets for plastics and biomass participated hybrid water electrolysis. *Chem Eng J.* 2023;465:142938. <https://doi.org/10.1016/j.cej.2023.142938>
 107. Wang H, Zhan W, Yu H, et al. Nitrogen-doped Ni₃P-NiMoO₄ heterostructure arrays for coupling hydrogen production with polyethylene terephthalate plastic electro-recycling. *Mater Today Phys.* 2023;37:101192. <https://doi.org/10.1016/j.mtphys.2023.101192>
 108. Mao Y, Fan S, Li X, et al. Trash to treasure: electrocatalytic upcycling of polyethylene terephthalate (PET) microplastic to value-added products by Mn_{0.1}Ni_{0.9}Co₂O_{4-δ} RSFs spinel. *J Hazard Mater.* 2023;457:131743. <https://doi.org/10.1016/j.jhazmat.2023.131743>
 109. Shi R, Liu K-S, Liu F, Yang X, Hou C-C, Chen Y. Electrocatalytic reforming of waste plastics into high value-added chemicals and hydrogen fuel. *Chem Commun.* 2021;57(94):12595-12598. <https://doi.org/10.1039/D1CC05032J>
 110. Li Y, Lee LQ, Yu ZG, et al. Coupling of PET waste electroreforming with green hydrogen generation using bifunctional catalyst. *Sustain Energy Fuels.* 2022;6(21):4916-4924. <https://doi.org/10.1039/D2SE01007K>
 111. Yang G, Jiao Y, Yan H, et al. Interfacial engineering of MoO₂-FeP heterojunction for highly efficient hydrogen evolution coupled with biomass electrooxidation. *Adv Mater.* 2020; 32(17):2000455. <https://doi.org/10.1002/adma.202000455>
 112. Li R-Q, Liu Q, Zhou Y, et al. 3D self-supported porous vanadium-doped nickel nitride nanosheet arrays as efficient bifunctional electrocatalysts for urea electrolysis. *J Mater Chem A.* 2021;9(7):4159-4166. <https://doi.org/10.1039/D0TA09473K>
 113. Li Y, Zhao Y, Zhao H, Wang Z, Li H, Gao P. A bifunctional catalyst of ultrathin cobalt selenide nanosheets for plastic-electroreforming-assisted green hydrogen generation. *J Mater Chem A.* 2022;10(38):20446-20452. <https://doi.org/10.1039/D2TA04286J>
 114. Maksoo I, Samanta RC, Zhan Y, Zhang K, Warratz S, Ackermann L. Polymer up-cycling by mangana-electrocatalytic C(sp³)-H azidation without directing groups. *Chem Sci.* 2023;14(30):8109-8118. <https://doi.org/10.1039/D3SC02549G>
 115. Grimaldos-Osorio N, Sordello F, Passananti M, Vernoux P, Caravaca A. From plastic-waste to H₂: electrolysis of a poly(methyl methacrylate) model molecule on polymer electrolyte membrane reactors. *J Power Sources.* 2020;480:228800. <https://doi.org/10.1016/j.jpowsour.2020.228800>
 116. Grimaldos-Osorio N, Sordello F, Passananti M, et al. From plastic-waste to H₂: a first approach to the electrochemical reforming of dissolved poly(methyl methacrylate) particles. *Int J Hydrogen Energy.* 2023;48(32):11899-11913. <https://doi.org/10.1016/j.ijhydene.2022.02.229>
 117. He W, Zhang J, Dieckhöfer S, et al. Splicing the active phases of copper/cobalt-based catalysts achieves high-rate tandem electroreduction of nitrate to ammonia. *Nat Commun.* 2022;13(1):1129. <https://doi.org/10.1038/s41467-022-28728-4>
 118. Liu Y, Liu K, Wang P, Jin Z, Li P. Electrocatalytic upcycling of nitrogenous wastes into green ammonia: advances and perspectives on materials innovation. *Carbon Neutrality.* 2023;2(1):14. <https://doi.org/10.1007/s43979-023-00055-7>
 119. Wang Z, Richards D, Singh N. Recent discoveries in the reaction mechanism of heterogeneous electrocatalytic nitrate reduction. *Catal Sci Technol.* 2021;11(3):705-725. <https://doi.org/10.1039/D0CY02025G>
 120. Theerthagiri J, Park J, Das HT, et al. Electrocatalytic conversion of nitrate waste into ammonia: a review. *Environ Chem Lett.* 2022;20(5):2929-2949. <https://doi.org/10.1007/s10311-022-01469-y>
 121. Yao Y, Wang J, Shahid UB, et al. Electrochemical synthesis of ammonia from nitrogen under mild conditions: current status and challenges. *Electrochem Energy Rev.* 2020;3(2):239-270. <https://doi.org/10.1007/s41918-019-00061-3>
 122. Ren T, Duan Z, Wang H, et al. Electrochemical co-production of ammonia and biodegradable polymer monomer glycolic acid via the co-electrolysis of nitrate wastewater and waste plastic. *ACS Catal.* 2023;13(15):10394-10404. <https://doi.org/10.1021/acscatal.3c02740>
 123. Hepburn C, Adlen E, Beddington J, et al. The technological and economic prospects for CO₂ utilization and removal. *Nature.* 2019;575(7781):87-97. <https://doi.org/10.1038/s41586-019-1681-6>
 124. Li J, Chen G, Zhu Y, et al. Efficient electrocatalytic CO₂ reduction on a three-phase interface. *Nat Catal.* 2018;1(8): 592-600. <https://doi.org/10.1038/s41929-018-0108-3>
 125. Zhang W, Hu Y, Ma L, et al. Progress and perspective of electrocatalytic CO₂ reduction for renewable carbonaceous fuels and chemicals. *Adv Sci.* 2018;5(1):1700275. <https://doi.org/10.1002/adv.201700275>
 126. Liu M, Pang Y, Zhang B, et al. Enhanced electrocatalytic CO₂ reduction via field-induced reagent concentration. *Nature.* 2016;537(7620):382-386. <https://doi.org/10.1038/nature19060>
 127. Kilaparathi SK, Addad A, Barras A, Szunerits S, Boukherroub R. Simultaneous upcycling of PET plastic waste and CO₂ reduction through co-electrolysis: a novel approach for integrating CO₂ reduction and PET hydrolysate oxidation. *J Mater Chem A.* 2023;11(47):26075-26085. <https://doi.org/10.1039/D3TA05726G>
 128. Ochedi FO, Liu D, Yu J, Hussain A, Liu Y. Photocatalytic, electrocatalytic and photoelectrocatalytic conversion of

- carbon dioxide: a review. *Environ Chem Lett.* 2021; 19(2):941-967. <https://doi.org/10.1007/s10311-020-01131-5>
129. Miao Y, Zhao Y, Waterhouse GIN, Shi R, Wu L-Z, Zhang T. Photothermal recycling of waste polyolefin plastics into liquid fuels with high selectivity under solvent-free conditions. *Nat Commun.* 2023;14(1):4242. <https://doi.org/10.1038/s41467-023-40005-6>
 130. Kim J, Jang J, Hilberath T, Hollmann F, Park CB. Photoelectrocatalytic biosynthesis fuelled by microplastics. *Nature Synthesis.* 2022;1(10):776-786. <https://doi.org/10.1038/s44160-022-00153-x>
 131. Bhattacharjee S, Rahaman M, Andrei V, et al. Photoelectrochemical CO₂-to-fuel conversion with simultaneous plastic reforming. *Nat Synth.* 2023;2:182-192. <https://doi.org/10.1038/s44160-022-00196-0>
 132. Li X, Wang J, Zhang T, Wang T, Zhao Y. Photoelectrochemical catalysis of waste polyethylene terephthalate plastic to coproduce formic acid and hydrogen. *ACS Sust Chem Eng.* 2022;10(29):9546-9552. <https://doi.org/10.1021/acssuschemeng.2c02244>
 133. Zhang B, Zhang H, Pan Y, et al. Photoelectrochemical conversion of plastic waste into high-value chemicals coupling hydrogen production. *Chem Eng J.* 2023;462:142247. <https://doi.org/10.1016/j.cej.2023.142247>
 134. Bhattacharjee S, Andrei V, Pornrunroj C, Rahaman M, Pichler CM, Reisner E. Reforming of soluble biomass and plastic derived waste using a bias-free Cu₃₀Pd₇₀|perovskite|Pt photoelectrochemical device. *Adv Funct Mater.* 2022;32(7):2109313. <https://doi.org/10.1002/adfm.202109313>
 135. Bellardita M, Loddo V, Parrino F, Palmisano L. (Photo)electrocatalytic versus heterogeneous photocatalytic carbon dioxide reduction. *ChemPhotoChem.* 2021;5(9):767-791. <https://doi.org/10.1002/cptc.202100030>
 136. Li X, Wang J, Sun M, Qian X, Zhao Y. Ti-Fe₂O₃/Ni(OH)_x as an efficient and durable photoanode for the photoelectrochemical catalysis of PET plastic to formic acid. *J Electrochem Soc.* 2023;78:487-496. <https://doi.org/10.1016/j.jechem.2022.12.031>
 137. Chen Z, Duan X, Wei W, Wang S, Ni B-J. Recent advances in transition metal-based electrocatalysts for alkaline hydrogen evolution. *J Mater Chem A.* 2019;7(25):14971-15005. <https://doi.org/10.1039/C9TA03220G>
 138. Wang Y, Liu K, Liu F, Liu C, Shi R, Chen Y. Selective electroreforming of waste polyethylene terephthalate-derived ethylene glycol into C₂ chemicals with long-term stability. *Green Chem.* 2023;25(15):5872-5877. <https://doi.org/10.1039/D3GC01486J>
 139. Chen Z, Zheng R, Graš M, et al. Tuning electronic property and surface reconstruction of amorphous iron borides via W-P co-doping for highly efficient oxygen evolution. *Appl Catal B Environ.* 2021;288:120037. <https://doi.org/10.1016/j.apcatb.2021.120037>
 140. Chen C, Kang Y, Huo Z, et al. Highly crystalline multimetallic nanoframes with three-dimensional electrocatalytic surfaces. *Science.* 2014;343(6177):1339-1343. <https://doi.org/10.1126/science.1249061>
 141. Zhang L, Zhao Z, Gong J. Nanostructured materials for heterogeneous electrocatalytic CO₂ reduction and their related reaction mechanisms. *Angew Chem Int Ed.* 2017;56(38):11326-11353. <https://doi.org/10.1002/anie.201612214>
 142. Voiry D, Chhowalla M, Gogotsi Y, et al. Best practices for reporting electrocatalytic performance of nanomaterials. *ACS Nano.* 2018;12(10):9635-9638. <https://doi.org/10.1021/acsnano.8b07700>
 143. Liu P, Chen B, Liang C, et al. Tip-enhanced electric field: a new mechanism promoting mass transfer in oxygen evolution reactions. *Adv Mater.* 2021;33(9):2007377. <https://doi.org/10.1002/adma.202007377>
 144. Wu Y-L, Li X, Wei Y-S, et al. Ordered macroporous superstructure of nitrogen-doped nanoporous carbon implanted with ultrafine Ru nanoclusters for efficient pH-universal hydrogen evolution reaction. *Adv Mater.* 2021;33(12):2006965. <https://doi.org/10.1002/adma.202006965>
 145. Li W, Liu J, Guo P, et al. Co/CoP heterojunction on hierarchically ordered porous carbon as a highly efficient electrocatalyst for hydrogen and oxygen evolution. *Adv Energy Mater.* 2021;11(42):2102134. <https://doi.org/10.1002/aenm.20210>
 146. Xiong P, Tan J, Lee H, et al. Two-dimensional carbon-based heterostructures as bifunctional electrocatalysts for water splitting and metal-air batteries. *Nano Mater Sci.* 2022. <https://doi.org/10.1016/j.nanoms.2022.10.001>
 147. Chen M, Zhang S-C, Zou Z-G, et al. Review of vanadium-based oxide cathodes as aqueous zinc-ion batteries. *Rare Met.* 2023;42(9):2868-2905. <https://doi.org/10.1007/s12598-023-02303-2>
 148. Chen Z, Duan X, Wei W, Wang S, Ni B-J. Electrocatalysts for acidic oxygen evolution reaction: achievements and perspectives. *Nano Energy.* 2020;78:105392. <https://doi.org/10.1016/j.nanoen.2020.105392>
 149. Sun J-P, Zheng Y, Zhang Z-S, Meng X-C, Li Z-Z. Modulation of d-orbital to realize enriched electronic cobalt sites in cobalt sulfide for enhanced hydrogen evolution in electrocatalytic water/seawater splitting. *Rare Met.* 2024;43(2):511-521. <https://doi.org/10.1007/s12598-023-02427-5>
 150. Yan N-F, Cui H-M, Shi J-S, You S-Y, Liu S. Recent progress of W₁₈O₄₉ nanowires for energy conversion and storage. *Tungsten.* 2023;5(4):371-390. <https://doi.org/10.1007/s42864-023-00202-8>
 151. Masnica JP, Sibte-e-Hassan S, Potgieter-Vermaak S, Regmi YN, King LA, Tosheva L. ZIF-8-derived Fe-C catalysts: relationship between structure and catalytic activity toward the oxygen reduction reaction. *Green Carbon.* 2023;1(2):160-169. <https://doi.org/10.1016/j.greenc.2023.11.001>
 152. Pham TA, Ping Y, Galli G. Modelling heterogeneous interfaces for solar water splitting. *Nat Mater.* 2017;16(4):401-408. <https://doi.org/10.1038/nmat4803>
 153. Xu Q, Zhang J, Zhang H, et al. Atomic heterointerface engineering overcomes the activity limitation of electrocatalysts and promises highly-efficient alkaline water splitting. *Energy Environ Sci.* 2021;14(10):5228-5259. <https://doi.org/10.1039/D1EE02105B>
 154. Li J, Pan W, Liu Q, et al. Interfacial engineering of Bi₁₉Br₃S₂₇ nanowires promotes metallic photocatalytic CO₂ reduction activity under near-infrared light irradiation. *J Am Chem Soc.* 2021;143(17):6551-6559. <https://doi.org/10.1021/jacs.1c01109>
 155. Liu J, Kargarian M, Kareev M, et al. Heterointerface engineered electronic and magnetic phases of NdNiO₃ thin films. *Nat Commun.* 2013;4(1):2714. <https://doi.org/10.1038/ncomms3714>

AUTHOR BIOGRAPHIES



Gaihong Wang received her Master degree at Nanjing Tech University in 2022. Now she is a Ph.D. student at the University of Technology Sydney. Her research work focuses on designing and synthesizing nanomaterials for electrochemical catalysis, aiming to develop sustainable energy solutions and address environmental challenges.



Zhijie Chen is a research associate at the University of New South Wales, Sydney. He received Ph.D. degree at the University of Technology Sydney in 2022. His research work focuses on the eco-design of nanomaterials for advanced energy/environmental applications.



Bing-Jie Ni received his Ph.D. degree in environmental engineering in June 2009. He currently is a full professor at the University of New South Wales, Sydney. He is a Fellow of the Royal Society of Chemistry and Clarivate Global Highly Cited Researcher. His work focuses on the integration of

different disciplines to develop innovative and sustainable technological solutions to achieve environmental and energy sustainability.

How to cite this article: Wang G, Chen Z, Wei W, Ni B-J. Electrocatalysis-driven sustainable plastic waste upcycling. *Electron.* 2024;2(2):e34. <https://doi.org/10.1002/elt2.34>